^{29}Si Solid-State NMR Analysis of Opal-AG, Opal-AN and Opal-CT: Single Pulse Spectroscopy and Spin-Lattice T_1 Relaxometry

Neville J. Curtis [1,2], Jason R. Gascooke [2,3], Martin R. Johnston [2,3,*] and Allan Pring [2,4]

1 South Australian Museum, North Terrace, Adelaide, SA 5000, Australia; neville.curtis@flinders.edu.au
2 College of Science and Engineering, Flinders University, Sturt Rd, Bedford Park, SA 5042, Australia; jason.gascooke@flinders.edu.au (J.R.G.); allan.pring@adelaide.edu.au (A.P.)
3 Institute for Nanoscale Science and Technology, Flinders University, Sturt Rd, Bedford Park, SA 5042, Australia
4 Department of Geology, School of Physical Sciences, University of Adelaide, Adelaide, SA 5005, Australia
* Correspondence: martin.johnston@flinders.edu.au; Tel.: +61-8-820-12317

Abstract: Single pulse, solid-state ^{29}Si nuclear magnetic resonance (NMR) spectroscopy offers an additional method of characterisation of opal-A and opal-CT through spin-lattice (T_1) relaxometry. Opal T_1 relaxation is characterised by stretched exponential (Weibull) function represented by scale (speed of relaxation) and shape (form of the curve) parameters. Relaxation is at least an order of magnitude faster than for silica glass and quartz, with Q_3 (silanol) usually faster than Q_4 (fully substituted silicates). 95% relaxation (Q_4) is achieved for some Australian seam opals after 50 s though other samples of opal-AG may take 4000 s, while some figures for opal-AN are over 10,000 s. Enhancement is probably mostly due to the presence of water/silanol though the presence of paramagnetic metal ions and molecular motion may also contribute. Shape factors for opal-AG (0.5) and opal-AN (0.7) are significantly different, consistent with varying water and silanol environments, possibly reflecting differences in formation conditions. Opal-CT samples show a trend of shape factors from 0.45 to 0.75 correlated to relaxation rate. Peak position, scale and shape parameter, and Q_3 to Q_4 ratios offer further differentiating feature to separate opal-AG and opal-AN from other forms of opaline silica. T_1 relaxation measurement may have a role for provenance verification. In addition, definitively determined Q_3/Q_4 ratios are in the range 0.1 to 0.4 for opal-AG but considerably lower for opal-AN and opal-CT.

Keywords: opal; hyalite; geyserite; silanol; solid-state NMR; silicon NMR; relaxation time; provenance

1. Introduction

Opal [1,2] is a generic term applied to commonly-found and naturally-formed hydrated silicas which lack the regular crystalline structure of quartz, moganite, cristobalite or tridymite [3]. X-ray powder diffraction (XRD) has been the primary method of classification [2] for over 50 years allowing delineation of opal-A (amorphous) comprising opal-AG (gel) and opal-AN (network, also known as hyalite), opal-CT (cristobalite/tridymite) and opal-C (cristobalite). Typically, XRD peaks are broad in all cases, particularly for opal-A [2,4–9], suggesting a disordered "paracrystalline" environment. Other variability, such as in the amount of molecular water [7,10–13], trace elements [14–22] and the mixture of silanols (Q_3 site with one oxygen as a silanol [23–25] with the remainder bridged to other silicon atoms) with fully substituted (Q_4 site all Si-O-Si bridged) species leads to a consensus that opal is not a true mineral. Despite extensive research, the structures of opal-A and opal-CT remain unresolved [3,12,26,27]. Opal-C shows similarities to cristobalite [2].

In terms of genesis, opal-AG primarily forms from ground waters associated with sedimentary rocks. Isotopic analysis of isotope signatures give temperature estimates below

45 °C [28]. "Play of colour" (POC) opal-CT is formed from low temperature hydrothermal fluids associated with volcanism while isotopic ^{18}O signatures and fluid inclusion studies give a range of temperatures from below 45 °C up to 190 °C [16,28–30]. Opal-AN (hyalite) is also associated with volcanic rocks, but is thought to form by vapor deposition from supercritical aqueous fluids under pressure at temperatures up to 400 °C [31]. This higher temperature of formation is consistent with lower water content than other opals with much believed to be present in the form of fluid inclusions. Opal-CT may deposit under ambient seepage [32] though some may be formed under volcanic conditions [28,33]. It is also proposed that there is a series of diagenetic transformations [12,34–40] from opal-AG through opal-CT to quartz and/or moganite. Opal-AN is not involved in this sequence.

We have recently undertaken a thorough re-examination of opal, using over 200 discrete specimens, both to investigate if those samples obtained from newer locations, such as Ethiopia and Madagascar, conform to the accepted classification [9] and to see if advanced modern techniques, such as specular and diffuse reflectance IR [41], can provide insights into the amorphous and paracrystalloid structures of opal-A and opal-CT. Despite a seeming similarity of chemical composition, identical XRD patterns and the for most part, common Raman and IR spectra, opal-AG and opal-AN differ both visibly and morphologically under the scanning electron microscope (SEM) where opal-AG displays a pattern of spheres while opal-AN shows no structure [41]. Previous work [41] has shown that the spectroscopic differences between the opal-AG and opal-AN may originate from the Q_3 rather than the Q_4 centres on the basis of slight differences in the minor Raman and IR peaks [41]. Other forms of opaline silica [2], such as geyserite, show the same XRD patterns as opal-AG and opal-AN but may again differ at the Q_3 focus. On the other hand, opal-CT and opal-A differ markedly in XRD patterns and Raman/IR spectra.

We now add a detailed solid-state ^{29}Si NMR study to provide further and distinct spectroscopic insights which may access different aspects of silica chemistry to those obtained by XRD, and Raman and IR spectroscopy. The work extends previous studies of opal [9,42–48], silica [44,48–55] and silicates [49,56–58] using our well-characterized reference sample set [9,41] and thus allows correlation with other techniques. Typical ^{29}Si NMR spectra of silicates show discrete, but not well separated pairs of peaks at −100 to −110 ppm and at −110 to −115 ppm, which have been ascribed to Q_3 and Q_4 centres respectively (see below). In this paper we examine single pulse (SP) ^{29}Si NMR to determine the fundamental spin-lattice (T_1) relaxation parameters and to explore trends within, and between, each opal type. The literature suggests a very long (typically thousands of seconds) spin-lattice (T_1) relaxation time for silicon nuclei in glass and quartz [48,51,54,59] while aluminosilicates exhibit a range of values, up to 5000 s for nacrite [60]. However, SP spectra have been reported for opal and there is no previous indication of any specific problems arising from slow relaxation, with T_1 values up to 10 s noted [42,46]. Of course, as for any study involving opal, such applicability needs to be tested against a range of types and specific specimens. The literature also suggests that as a spin-dilute [61] system, opal may follow a stretched exponential [61–64] regime (Weibull parameters) of relaxometry, as opposed to a simple exponential.

2. Materials and Methods

A wide range of opals was sourced from museum collections and recent acquisitions [9,41] with types, locations and sample description given in Appendix A. All samples have been classified by XRD [2] and none contain more than a trace of quartz. Some samples contain clearly different zones within the same piece and are marked as such. Specimens G13767, G34996 and G34997 all comprise different pieces collected from the same location. The former comprises seam opal-AG samples from Lightning Ridge, New South Wales and are identified by physical appearance. The latter two are mixed assemblages of fossilized molluscs from Coober Pedy, South Australia and have no obvious differentiating features other than species. Two samples of mussels are labelled G34996 (1) and (2), while G34997 (1), (2) and (3) refer to three examples of belemnites. One piece from

G34997 showed sharp peaks in the XRD pattern due to minor clay inclusions. Possibly it derives a coating material on the fossil. There were no obvious peaks in the NMR spectrum associated with inclusions [65]. For brevity, Australian samples are classified by state (e.g., South Australia). Samples were finely ground in a tungsten carbide mortar and pestle and were stored in lightly sealed vials. For other analytical techniques involving opal, suitable quantity, and the ability to conduct destructive testing, limited the availability of samples.

Two samples were sourced from Caldes de Malavella in Catalonia, Spain and labelled "menilite" (from the Camp del Ninots [66] and popularly called "ninots") but are opal-A by XRD, with small amounts of quartz, and are distinct from a South Australian Museum specimen labelled as from Ménilmontant in France, which is opal-CT. These show spheres under the SEM [41] but these are not regularly arranged as, for instance POC Australian opal-AG samples. We refer to these as "Spanish menilite". Spectral evidence [41] suggest that these, geyserites (from Rotorua in New Zealand) and a sample labelled "hydrophane" opal from Dubnik in Slovakia, may be differentiated from opal-AG and opal-AN according to minor Raman peaks [41]. A sample of Gilson synthetic opal was acquired about 30 years ago by the South Australian Museum. A range of opal-CT samples covering progressively more complex XRD patterns was selected [9].

The minor and trace metal ion content of gem opals has been extensively analyzed for provenance reasons [16] or to explore diagenesis [20,21,67] while less attention has been paid to hyalites (opal-AN). Laser ablation/ion coupled plasma elemental analyses of selected samples (see Appendix B and Supplementary Materials) were conducted at Adelaide Microscopy using an Agilent 7900x (Agilent, Santa Clara, CA, USA) with attached New Wave NWR213 laser ablation system with NIST612 (primary for calibration and drift correction) and NIST614 (secondary) standards. A 10 ms dwell time was used for each spot and the calibration was undertaken every after every 15 point analyses. Results are presented as the average of at least 5 measurements in different positions. Data were processed using LADR software (Norris Scientific) and standard reference values from the GeoREM database [68]. Trace elements were quantified by normalizing to 75 weight% oxide totals (~35 weight% Si), which assumed 25 weight% H_2O content in each opal. This approximation will have a minor effect on the values presented here.

NMR experiments were undertaken using a Bruker Avance III 400 MHz spectrometer (Bruker, Billerica, MA, USA) operating at 79.5 MHz for ^{29}Si. Chemical shifts are relative to powdered DSS (sodium 3-(trimethylsilyl)propane-1-sulfonate or 2,2-dimethyl-2-silapentane-5-sulphonic acid sodium salt) at 0 ppm. Solid DSS is the current preferred external standard [69] for solid-state Si NMR rather than the liquid tetramethylsilane (TMS) which requires a sealed insert for use of a liquid. When compared DSS was found at +1.53 ppm relative to liquid TMS at 0 ppm [70]. T_1 relaxation time experiments were carried out using a saturation-recovery technique with a range of recycle delays, with decoupling during acquisition, befitting the large values being determined [71]. Approximately 100 mg of finely ground opal sample was placed in a Bruker 4 mm rotor and spun at 5 kHz. 90° Pulse length was 5 μs for ^{29}Si and acquisition times were typically 12 ms. Typically, 140–200 scans per delay were recorded giving suitable signal to noise ratio. A range of delay times spanning 0–400 s was employed. After some experimentation the delays used were 1, 2, 3, 5, 7, 10, 15, 20, 25, 35, 50, 75, 100, 200 and 400 s in addition to the zero-time value. Longer delay times are impractical as the 400 s experiment delay time experiment required almost 20 h of collection alone.

Unetched SEM images were obtained using a FEI Inspect 50 SEM (FEI, Hillsboro, ND, USA) by recording the secondary electron emission at an acceleration voltage of either 5 or 10 kV and working distances of 4 to 6 mm. Samples were sputter coated with a 2 nm layer of Pt.

All samples were measured under ambient atmospheric conditions. N_2 flushing experiments were carried out using a small amount of finely ground opal sample in a sample vial placed under a blanket of nitrogen for minimum of 2–3 days. These flushed samples were transferred to the solid-state rotor using an inverted filter funnel dispensing

nitrogen over the filling apparatus. Samples were then run immediately in T_1 determination experiments. A rigorous freeze-thaw process was not undertaken due to concerns about the possible effect of dehydration [72] on the system.

We verified that the Weibull cumulative density function relationship, variously described as the Kohlrausch function, Williams-Watts equation or stretched exponential [61–63,73] Equation (1), gave the best fits for the growing development of signal with time, $A(t)$.

$$A(t) \; = \; A_\infty \left(1 - \exp \left(- \left(\frac{t}{\lambda} \right)^{\kappa} \right) \right) \tag{1}$$

In this, A_∞ is the signal at infinite time, t represents the delay time, λ represents a time related scale parameter while κ is termed the shape parameter. This shape factor defines how far removed the curve is from an exponential, with a value of 0.5 more different than 0.7. Only in the special case of $\kappa = 1$ does the curve become an exponential and Equation (1) becomes the more familiar form in Equation (2) where T_1 is the conventional relaxation time. In this paper, we use the term T_1 to indicate focus on the longitudinal spin-lattice relaxation process rather than the transverse T_2 spin-spin process.

$$A(t) \; = \; A_\infty \left(1 - \exp \left(- \left(\frac{t}{T_1} \right) \right) \right) \tag{2}$$

Initially, all samples were analyzed to ensure they followed a Weibull form by fitting each spectrum to two Gaussian functions where the same Q_3 and Q_4 positions and full width half maxima (FWHM) were used for each spectrum in a time-delay series. The peak areas were fitted to Equation (1) and in all cases good fits were obtained and always with $\kappa < 1$ meaning the signal rises faster than an exponential at early times and slower to asymptote to the infinite-time value. No samples showed an exponential relationship. Final κ and λ values for a sample were determined by simultaneously refitting all the spectra in the time-delay series to 10 variables: peak position, FWHM, final (infinity) signal level, and shape and scale parameters for both Q_3 and Q_4 components. This involved over 10,000 data points in the range −80 to −130 ppm from 1 to 400 s delay times. Scale parameters are quoted to 3 significant figures with fitting uncertainties determined from the non-linear least squares algorithm [74]. Shape parameter uncertainties are listed to two decimal places, though in many cases the uncertainty is much lower than the default minimum of ±0.01. The ratios of the final areas for the Q_3 and Q_4 peaks were used to estimate the respective proportions of the two components with the quoted ±0.01 uncertainty value determined to be the upper limit. Q_3/Q_4 ratios were determined using final (A_∞) signal levels for the two peaks.

3. Results

Saturation of the ^{29}Si NMR signal followed by a variable delay time allows the excited nuclei to return to the ground state and signal intensity to return. As a variety of behaviours was seen, we address each opal "type" in turn, using the arbitrary delineation given in Table 1 (opal-A) and Table 2 (opal-CT). Full, or mostly complete, relaxation is evidenced by a flattening of the intensity versus time curve, or minor intensity increases between delay time spectra. As can be seen (Figure 1) relaxation is largely complete after 400 s delay time for the example of opal-AG shown but is only partial for an opal-AN specimen.

Table 1. Weibull fitting: scale parameter (λ) and shape parameter (κ) for opal-A specimens with extrapolated Q_3 to Q_4 ratios. One standard deviation fitting errors are given. Sources given in Appendix A.

	Q_3 λ (s)	Q_3 κ	% Q_3 Relaxation after 400 s	Q_4 λ (s)	Q_4 κ	% Q_4 Relaxation after 400 s	Q_3/Q_4 Ratio
Australian seam opal							
G1401	6.48 ± 0.05	0.51 ± 0.01	>99	7.43 ± 0.01	0.51 ± 0.01	>99	0.24 ± 0.01
G1442	5.71 ± 0.06	0.49 ± 0.01	>99	5.94 ± 0.02	0.51 ± 0.01	>99	0.38 ± 0.01
G7682	6.64 ± 0.13	0.43 ± 0.01	>99	9.37 ± 0.1	0.45 ± 0.01	>99	0.18 ± 0.01
G8608	11.1 ± 0.1	0.59 ± 0.01	>99	18.1 ± 0.1	0.51 ± 0.01	99	0.33 ± 0.01
G9258	8.88 ± 0.12	0.47 ± 0.01	>99	8.40 ± 0.02	0.49 ± 0.01	>99	0.28 ± 0.01
G9592	21.6 ± 0.3	0.57 ± 0.01	>99	33.3 ± 0.1	0.53 ± 0.01	98	0.21 ± 0.01
G9811	7.15 ± 0.05	0.49 ± 0.01	>99	9.92 ± 0.03	0.51 ± 0.01	>99	0.49 ± 0.01
G13767 [a,b]	3.85 ± 0.05	0.52 ± 0.01	>99	4.80 ± 0.01	0.51 ± 0.01	>99	0.24 ± 0.01
G13767 [a,c]	4.69 ± 0.06	0.47 ± 0.01	>99	5.54 ± 0.02	0.50 ± 0.01	>99	0.28 ± 0.01
GNEW22	5.05 ± 0.06	0.47 ± 0.01	>99	4.95 ± 0.01	0.52 ± 0.01	>99	0.32 ± 0.01
GNEW31	4.00 ± 0.04	0.55 ± 0.01	>99	5.00 ± 0.01	0.47 ± 0.01	>99	0.18 ± 0.01
T2233	5.04 ± 0.06	0.46 ± 0.02	>99	4.92 ± 0.01	0.52 ± 0.10	>99	0.32 ± 0.01
G1401 [d]	11.4 ± 0.3	0.38 ± 0.01	>99	7.17 ± 0.02	0.50 ± 0.01	>99	0.18 ± 0.01
G8608 [d]	14.1 ± 0.2	0.55 ± 0.01	>99	18.9 ± 0.4	0.50 ± 0.01	99	0.26 ± 0.01
Queensland boulder opal							
G7532	66.9 ± 1.5	0.61 ± 0.01	95	122 ± 1	0.53 ± 0.01	85	0.20 ± 0.01
WBO1	157 ± 6	0.73 ± 0.01	86	910 ± 36	0.69 ± 0.01	43	0.12 ± 0.01
Coober Pedy (Australia) opalised molluscs							
G34996 [a] (1)	22.2 ± 0.3	0.50 ± 0.01	>99	23.8 ± 0.1	0.53 ± 0.01	>99	0.26 ± 0.01
G34996 [a] (2)	18.9 ± 0.3	0.51 ± 0.01	>99	19.6 ± 0.01	0.54 ± 0.01	>99	0.27 ± 0.01
G34997 [a] (1)	49.3 ± 1.2	0.54 ± 0.01	96	50.9 ± 0.2	0.52 ± 0.01	95	0.18 ± 0.01
G34997 [a] (2)	30.4 ± 0.6	0.50 ± 0.01	97	33.2 ± 0.1	0.52 ± 0.01	97	0.23 ± 0.01
G34997 [a] (3)	25.2 ± 0.4	0.53 ± 0.01	99	32.2 ± 0.1	0.52 ± 0.01	98	0.28 ± 0.01
Slovakian opals							
SO3	31.7 ± 0.5	0.56 ± 0.01	99	136 ± 2	0.44 ± 0.01	80	0.24 ± 0.01
SO7	28.9 ± 0.3	0.57 ± 0.01	97	40.4 ± 0.1	0.56 ± 0.01	96	0.20 ± 0.01
SO17	16.5 ± 0.7	0.41 ± 0.01	99	31.0 ± 0.2	0.47 ± 0.02	85	0.15 ± 0.01
G34280	66.2 ± 0.5	0.82 ± 0.01	99	154 ± 2	0.68 ± 0.01	85	0.76 ± 0.01
Spanish menilites (Camp del Ninots)							
GNEW01	88.4 ± 4.1	0.61 ± 0.01	92	3730 ± 590	0.50 ± 0.01	28	0.15 ± 0.01
GNEW23	325 ± 38	0.61 ± 0.01	62	>10,000 [g]	0.50 ± 0.01	- [g]	- [g]
Hydrophane (Slovakia)							
G34475 [e]	7.89 ± 0.09	0.56 ± 0.01	>99	21.7 ± 0.1	0.49 ± 0.01	98	0.21 ± 0.01
G34475 [f]	42.5 ± 1.0	0.54 ± 0.01	96	118 ± 1	0.49 ± 0.02	84	0.18 ± 0.01
Opal-AN (worldwide)							
E1937	113 ± 2	0.84 ± 0.01	94	1480 ± 60	0.70 ± 0.01	33	0.09 ± 0.01
G8877	224 ± 16	0.77 ± 0.01	79	2390 ± 160	0.67 ± 0.01	26	0.07 ± 0.01
G32740	98.2 ± 1.7	0.88 ± 0.01	97	2490 ± 130	0.63 ± 0.01	27	0.07 ± 0.01
M8736	126 ± 3	0.83 ± 0.01	93	>10,000 [g]	0.65 ± 0.01	- [g]	- [g]
MS-4	105 ± 3	0.76 ± 0.01	92	2470 ± 130	0.67 ± 0.01	26	0.06 ± 0.01
OOC10	99.6 ± 3.0	0.86 ± 0.01	96	2510 ± 160	0.57 ± 0.01	30	0.05 ± 0.01
T18117	83.4 ± 0.8	0.85 ± 0.01	98	371 ± 5	0.79 ± 0.01	65	0.20 ± 0.01
T18511	96.0 ± 4.0	0.90 ± 0.02	97	1050 ± 80	0.62 ± 0.01	42	0.06 ± 0.01
Geyserites (New Zealand)							
G21471	81.8 ± 0.9	0.80 ± 0.01	97	237 ± 2	0.70 ± 0.01	76	0.22 ± 0.01
T1665	67.6 ± 0.5	0.79 ± 0.05	98	172 ± 2	0.72 ± 0.01	83	0.63 ± 0.01
Synthetic opal							
Gilson	97.6 ± 3.2	0.73 ± 0.01	94	1550 ± 60	0.60 ± 0.01	36	0.06 ± 0.01

[a] different specimen from a collection of samples [b] pale glass [c] orange glass [d] nitrogen flushing experiment [e] opaque zone [f] translucent zone [g] Unreliable values, see text.

Table 2. Weibull fitting: scale parameter (λ) and shape parameter (κ) for opal-CT with extrapolated Q_3 to Q_4 ratios. One standard deviation fitting errors are given. Sources given in Appendix A.

	Q_3			Q_4			
	λ (s)	κ	% Relaxation after 400 s	λ (s)	κ	% Relaxation after 400 s	Q_3/Q_4 Ratio
G1421	83.9 ± 4.4	0.68 ± 0.01	94	936 ± 50	0.66 ± 0.02	43	0.07 ± 0.01
G9942	89.1 ± 4.8	0.65 ± 0.01	93	>3000	0.56 ± 0.01	27	0.04 ± 0.01
G13755	29.5 ± 3.6	0.42 ± 0.02	95	311 ± 7	0.54 ± 0.01	68	0.06 ± 0.01
G13761	35.2 ± 2.5	0.52 ± 0.02	97	129 ± 1	0.54 ± 0.01	84	0.05 ± 0.01
G32925	87.8 ± 1.5	0.82 ± 0.01	97	710 ± 23	0.73 ± 0.01	48	0.14 ± 0.01
GNEW05	- [a]	- [a]	- [a]	21.1 ± 0.2	0.47 ± 0.01	98	- [a]
GNEW08	93.2 ± 15.7	0.48 ± 0.02	87	226 ± 5	0.46 ± 0.01	73	0.05 ± 0.01
GNEW09	87.6 ± 1.7	0.86 ± 0.01	98	566 ± 17	0.75 ± 0.01	54	0.13 ± 0.01
GNEW19	86.8 ± 3.1	0.79 ± 0.01	96	1820 ± 130	0.67 ± 0.01	30	0.06 ± 0.01
GNEW20	69.2 ± 2.3	0.64 ± 0.01	95	485 ± 11	0.53 ± 0.01	59	0.08 ± 0.01
GNEW24	19.8 ± 0.7	0.58 ± 0.01	>99	67.8 ± 0.5	0.52 ± 0.01	92	0.07 ± 0.01
GNEW27	- [a]	- [a]	- [a]	398 ± 12	0.54 ± 0.01	63	- [a]
GNEW28	32.6 ± 0.2	0.45 ± 0.01	96	81.3 ± 13.8	0.42 ± 0.01	86	0.09 ± 0.01
GNEW30	54.3 ± 1.3	0.87 ± 0.01	>99	962 ± 44	0.70 ± 0.01	42	0.06 ± 0.01
M53441	59.7 ± 1.8	0.83 ± 0.01	99	879 ± 44	0.68 ± 0.01	44	0.06 ± 0.01
NMNH Eth S2	91.0 ± 1.9	0.61 ± 0.01	92	371 ± 9	0.62 ± 0.01	65	0.45 ± 0.01
OOC3	76.8 ± 4.6	0.64 ± 0.01	94	212 ± 5	0.55 ± 0.01	76	0.09 ± 0.01
OOC5	108 ± 7	0.55 ± 0.01	87	1100 ± 50	0.63 ± 0.01	41	0.09 ± 0.01
T4051	115 ± 3	0.74 ± 0.01	92	642 ± 19	0.63 ± 0.01	52	0.15 ± 0.01
T22842	54.8 ± 8.8	0.43 ± 0.02	*92*	109 ± 1	0.50 ± 0.01	52	0.06 ± 0.01

[a] Unreliable λ value, see text.

First, we consider an Australian seam opal-AG (Figure 1a) where there is an asymmetric peak which can be interpreted as overlapping Q_3 and Q_4 components [46]. This asymmetry, rather than separated peaks, has been noted before [42,43]. Q_3 peaks can be fitted giving values spanning −104 to −107 ppm (FWHM typically 5 ppm) with the range probably caused by the lack of a clear peak, or shoulder. In common with the other opals, the major Q_4 peak is at −113 to −114 ppm (FWHM about 4 ppm). The Q_3 to Q_4 ratio was 0.38 and was deduced from extrapolations to infinite time (inset) and these accord with visual observation and fitting of the 400 s delay time spectra. Other samples are in the range 0.2 to 0.5. Relaxation times are relatively fast in comparison with the other opal-A samples even for other examples of opal-AG. Shape factors are routinely about 0.5, both for Q_3 and Q_4.

Opal-AN (Figure 1b) samples present different ^{29}Si NMR spectra to those for opal-AG with a more separated pair of peaks, again ascribable to Q_3 and Q_4. The plots are however of poorer quality, possibly as a result of the slower relaxation time. Curve-fitting gives Q_3 at −103 to −104 ppm (FWHM typically 4 ppm) and −113 to −114 ppm (FWHM typically 4 ppm) for Q_4. Although several of the examples are only partially relaxed after 400 s delay time, the data shows a general trend to a lower ratio of Q_3 to Q_4 than for opal-AG, in the range 0.05 to 0.20 (Table 1). Q_3 scale factors show slower relaxation than for opal-AG and scan the range of about 100 to 200 s while those for Q_4 are far slower and more variable. As can be seen (Table 1) even for the fastest relaxation (T18117 from N. Carolina, USA), as shown in Figure 1b, only 60% relaxation of Q_4 is achieved after 400 s delay time, with many much less. It would be impractical to gain more extensive scale factor data as the individual experimental times might run to several weeks. Thus, some of the slower Q_4 scale factors should be treated as indicative only. However, the shape factors are more robust and show values of about 0.7 to 0.8 for both Q_3 and Q_4. For the example shown in Figure 1b, the ratio of Q_3 to Q_4 decreases from 0.54 after 10 s delay time, to 0.30 after 400 s and 0.20 at infinite time (see [48]) illustrating the need for extrapolated final values. This bias leads to a reliable determination of the Q_3 parameters even though the percentage

is low. The differences in shape factors between the opal-AG (typically 0.5) and opal-AN (typically 0.7) are consistent within each type.
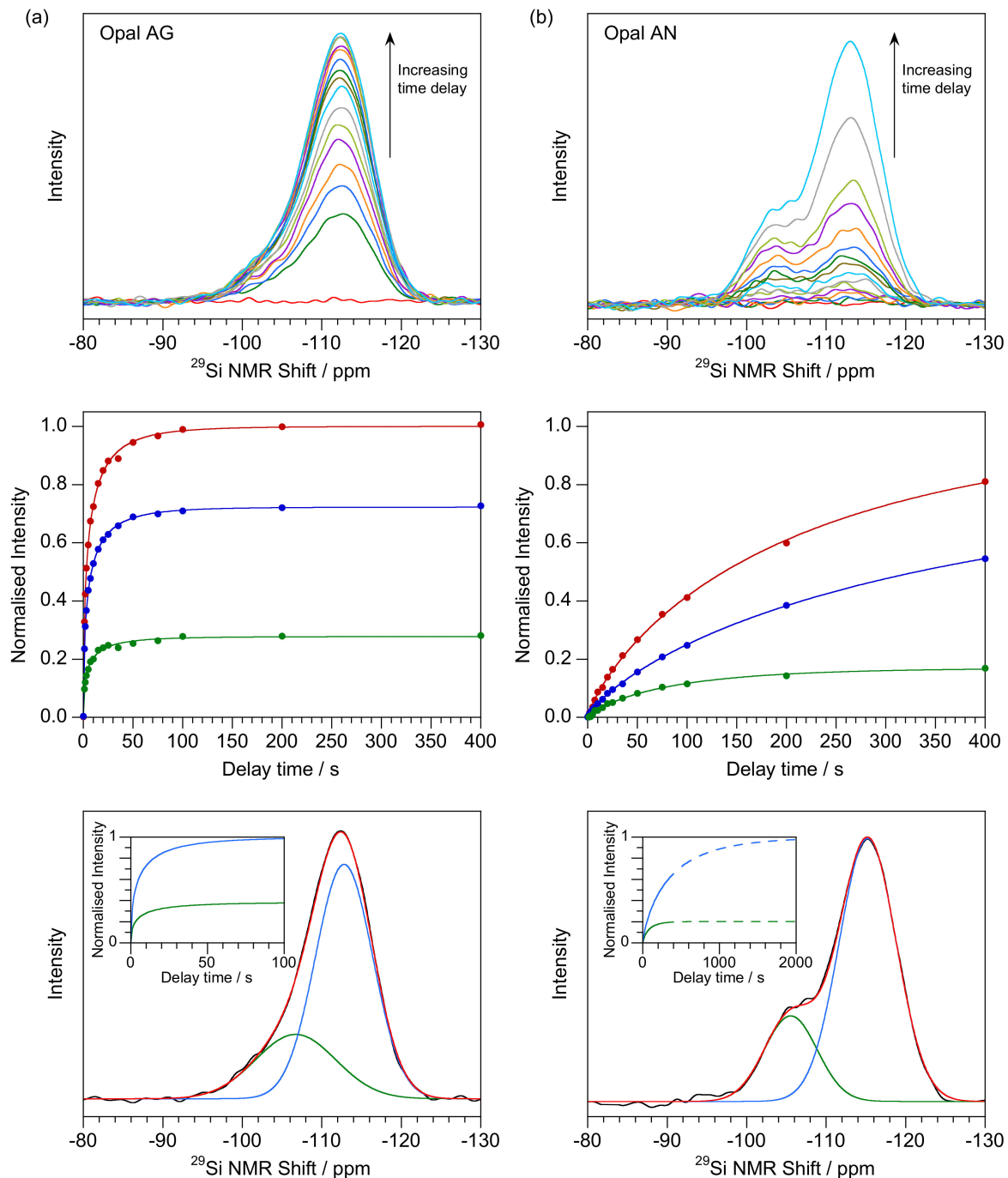
Figure 1. Side by side comparison of (**a**) Opal-AG (G1442 from William Creek, South Australia) with (**b**) Opal-AN (T18117 from North Carolina, USA). Top: spectra after delay times of 1, 2, 3, 5, 7, 10, 15, 20, 25, 35, 50, 75, 100, 200 and 400 s (with the zero-time measurement shown in red). Middle: Time dependence of the total integrated signal (red), and Gaussian-fitted Q_3 (green) and Q_4 (blue) signals. The line of best fit from Weibull fitting is shown as solid line. Intensity is normalized to the fitted A_∞ value of the integrated signal fit. Lower: Gaussian deconvolution of the Q_3 and Q_4 components for the 400 s delay time data as determined from global fit of all delay times. The time behaviour displayed in the inset is generated from the globally fitted λ and κ values and normalized to the Q_4 A_∞ value. Extrapolated data to longer times is shown by a dashed line.

Details for other examples of opal-A are given in Table 1 with some plotted in Supplementary Materials. Some of these samples show relatively short relaxation times though there is a large range of values. For instance, Queensland boulder opals and opal-AG samples from Slovakia show slower relaxation than the Australian seam opals though mostly have similar Q_3 to Q_4 ratios. The two examples of "Spanish menilite" (Supplementary Materials), however, relaxed very slowly and may contain low Q_3 levels. Other fine, and potentially informative, detail is revealed in this work. For instance, the opalised molluscs show moderately fast relaxation but have similar parameters for Q_3 and Q_4 unlike other examples where the difference ranges from minor (for fast T_1 relaxation) to over a factor of five (for slower relaxation). This was verified through examination of several distinct samples. Two visually distinct zones of the hydrophane example, G34775 (Supplementary Materials), show different scale parameters though similar shape values. The final extrapolated Q_3 to Q_4 parameter suggest a similar silica composition. The spectrum for a sample of Gilson synthetic opal (Supplementary Materials) shows clear evidence for a peak at -103 to -104 ppm (FWHM about 3–4 ppm) which is more separated than for the other opal-AG samples. Significantly, the scale and shape parameters lie between those for opal-AG and opal-AN. Curve fitting suggested a relatively low proportion of Q_3, while Q_4 showed slow relaxation. For reference, the XRD pattern (broad peak centered at 4.0 Å [9]), IR spectrum (wide peak at 800 cm^{-1} and shoulder at 550 cm^{-1} [41]) and Raman (broad peak 300–500 cm^{-1} [9]) are all consistent with opal-A.

The spectra (Figure 2) for the New Zealand geyserites, on the other hand, are more like opal-AN than opal-AG, showing more resolved Q_3 and Q_4 peaks with shape factors of 0.7 to 0.8. Both samples can be fitted to two peaks at -103 to -105 ppm and -113 ppm with FWHM in the range 3–5 ppm. While the Q_3 to Q_4 ratio in G21471 was about 0.2 it was much higher for T1665 (Table 1) though both shared the same shape parameters.
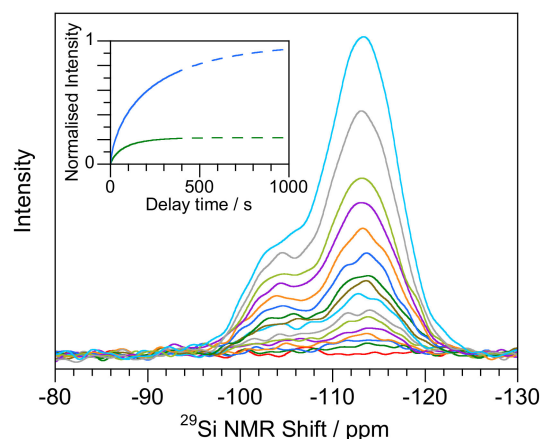
Figure 2. (main) Evolution of signal with delay time for geyserite (G21471 from Rotorua, New Zealand). Delay times are 1, 2, 3, 5, 7, 10, 15, 20, 25, 35, 50, 75, 100, 200 and 400 s (with the zero-time measurement shown in red) (insert) calculated fitting of Q_3 (green) and Q_4 (blue) components using data in Table 2 scaled to Q_4 maximum.

Opal-CT samples show spectra ranging from those with a prominent presumed Q_3 peak (Figure 3a) to examples where the peak (Figure 3b) is minor. An example of each type has been reported previously [43,46]. Figure 3 shows the differences in fitted spectra and relaxation times between the two. Shape factors span the range between those found for opal-AG and opal-AN. Q_4 data shows that relaxation is often less than 50% after 400 s delay time. The highest Q_3 to Q_4 ratios are only 0.15 (Table 2) for opal-CT with many much smaller. Solutions show maxima at about -104 to -105 (Q_3) and -113 to -114 ppm (Q_4) with FWHM of about 3 ppm for both peaks. The marginally narrower FWHM (when compared to opal-AG) for the presumed Q_3 peak at around -104 ppm gives a visual appearance for G32925 more like opal-AN than opal-AG.
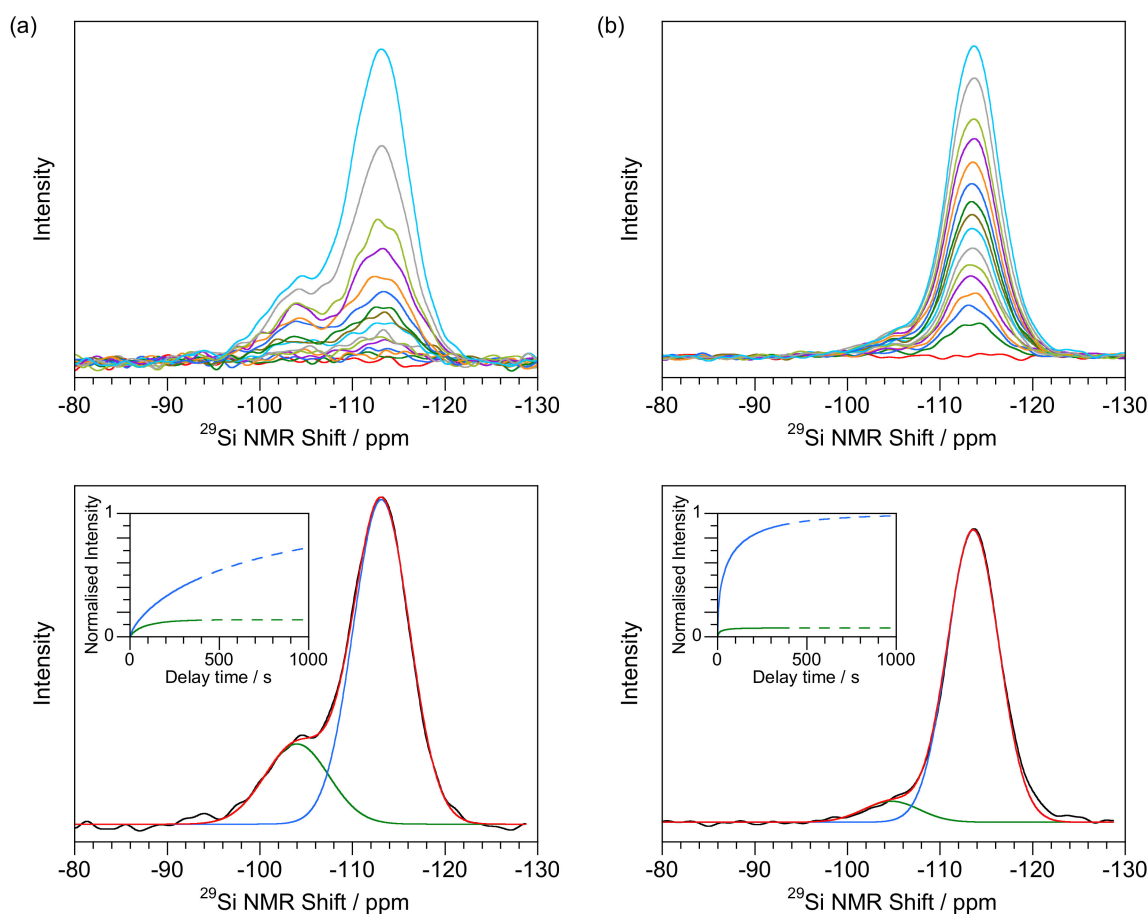
Figure 3. Evolution of signal with delay time for opal-CT (**a**) with a separated Q_3 peak (G32925 from Zelinograd, Qazaqstan) (**b**) less delineated Q_3 peak (GNEW24 from Kutahuya, Turkey). Top: spectra after delay times of 1, 2, 3, 5, 7, 10, 15, 20, 25, 35, 50, 75, 100, 200 and 400 s (with the zero-time measurement shown in red). Lower: Q_3 (green) and Q_4 (blue) fitting for the 400 s delay time data with infinite time extrapolated data shown in inset.

Curve fitting for NMNH Eth S2 (bottle-glass brown opal-CT with POC from Ethiopia) gave what appeared to be anomalous results. The main peak was broad and asymmetric while the computed solution gave a Q_3 to Q_4 ratio of 0.45 with the presumed Q_3 peak at −109.0 ppm (FWHM 7 ppm) with Q_4 at the consistent position of −114.2 (FWHM 3 ppm). At −109 ppm, the Q_3 peak position was considerably removed from other samples. The visual appearance does however suggest a high level of Q_3 (see later) while the shape and scale factors seem credible.

Full curve-fitting was not successful in all cases with problems encountered for the Q_3 components of GNEW05 and GNEW27. Both fitting solutions showed λ values greater than for Q_4 and κ terms of about 0.4 though both with very high fitting errors. We believe that there is a trade-off between the shape and scale parameters that the fitting algorithm is unable to resolve for these minor peaks. This results in artificially high and low values for the respective terms. The Q_4 terms seemed consistent though GNEW05 shows very fast relaxation. In another case, GNEW03 (opaque green sample from Mt Iyobo, Tanzania) gave an anomalous spectrum including what looked like two peaks at around −113 ppm. Combined Q_3 and Q_4 gave respective λ and κ values of 23 s and 0.50. XRD shows a possible minor silicate impurity at 4.45 Å which might lead to a more complex NMR spectrum.

4. Discussion

4.1. ^{29}Si NMR Spectra of Opal

Opal spectra [42–48] should be interpreted in relation to well-characterized polymorphs of silica, such as coesite [50], cristobalite [43,49,50], tridymite [43,50], moganite [75], quartz [43,44,49,50,59] as well as less structurally defined materials including glass [51] and volcanic sinters [48] noting the importance of systematic referencing of chemical shifts. There is general support that the major peak in opal [42–48] is due to the fully silicate bridged Q_4. In our work, we find that the major peaks are about 5 ppm more negative than quartz, consistent with previous work though at different absolute values probably caused by the use of external standards (we use DSS), experimental variations and differences in natural materials. We found kaolinite at −92.76 ppm and quartz (150 s delay time) at −108.64 ppm (FWHM of 1.2 ppm) relative to DSS at 0 ppm. Other authors have reported the quartz signal in the range −107.1 to −107.4 [43,44,49,50,59]. This difference is consistent with the offset value of about +1.5 ppm between DSS and TMS [70] (see before). The major peaks consistently lie in the range −113 to −114 ppm for all samples of opal-AG, opal-AN and opal-CT with little difference between type as noted before [44]. The variations in reported absolute values make any comparison of opal (this work) to previous work on silica polymorphs, such as tridymite or cristobalite, difficult. We also note the importance of conducting any comparative solid-state Si NMR study by using a clearly defined calibration in the instrument. None of the samples studied here contain evidence for cristobalite by XRD or Raman and IR spectroscopy. In addition, as will be described below, the relative proportions of Q_3 and Q_4 also affect the peak positions, particularly the latter.

Peaks due to silanol (Q_3) in opal-A and opal-CT are expected at less negative chemical shifts than for Q_4 and have been observed in varying amounts in previous work [44–46] usually as shoulders in SP spectra. They are also prominent in ^{1}H-^{29}Si cross polarization (CP) NMR spectra [44–47]. There is other spectroscopic evidence through mid-IR and mid-Raman [41] and near-IR [23–25] spectra which show silanol hydroxyls in addition to water. In the present work these peaks are mostly in the range −104 to −107 ppm.

We found Q_3 to Q_4 ratios generally in the range 0.05 to 0.3 with opal-AG showing more silanol than opal-AN and opal-CT. These figures are compatible with the 19–23% abundance of Q_3 reported [45,47] through curve-fitting. However, it has been proposed that this figure may be artificially high [48] with a lower figure of 10% proposed for opal-AN and 13–15% for Yellowstone geyserites. The use of the extrapolated infinite time signal value, however, as detailed in this work, provides a novel and definitive method for estimation of this ratio. Simple calculations suggest that, for instance, a 0.3 ratio of Q_3 to Q_4 would equate to a weight percentage of about 3.3% "water" present as $(SiO)_3Si$-OH HO-$Si(OSi)_3$ (compare with $(SiO)_3Si$-O-$Si(OSi)_3$). Of course, free water is also present in fluid inclusions and possibly as non-structural water of hydration [7,10,23,76]. Even a low figure of 1% water all present as silanol would result in a ratio of 0.07 Q_3 to Q_4. Similarly, a figure of 7% water would lead to a ratio of 1:1 Q_3 to Q_4. Other techniques give results in this range (e.g., [12]) with values up to 16% water being reported though with no correlations between opal types.

We also note that the spectrum will be more complicated than a simple mix of single Q_3 and Q_4 peaks. If Q_3 is present, then this is likely to cause a disruption of the silicate rings and sheets allowing geometric effects. Each Q_4 SiO_4 tetrahedra is linked to 4 other Si ions via bridging oxygens, as nearest cation neighbors. These Si ions are in turn linked to 3 further Si ions, so there may be 10 to 12 Si ions in the second cation coordination sphere. The number of Si in the second cation co-ordination sphere depends on the structural topology, if a 3-dimensional framework it will be 12. Different types of, and adjacent Q_3 sites, would also produce subtle differences in the spectrum. Similarly, the effect of tetrahedral Al^{3+} [47] may also produce additional peaks if it substitutes for Si^{4+}. Finally, both Q_3 and Q_4 may be subject to water proximity effects which although unlikely to have a major effect on chemical shift, will make a profound difference in the appearance of both the SP and ^{1}H-^{29}Si CP spectra, particularly in the relative magnitudes of the peaks. Given

the relatively high level of Q_3 in opal-AG this species is likely to have the most complicated spectra and may require extensive further analysis, such as CP studies, to resolve.

There is also no reason to suppose absolute structural homogeneity in opals and Q_3 to Q_4 ratios may vary within each opal type and even with samples taken from a single specimen. This would result in subtly different maxima for the main peaks as a result of different composition or the extent to which the Q_3 and Q_4 centres have relaxed. For instance, changes in peak position have been seen for silica glass with differing measurement delay times [49]. The evidence from this work, given FWHM of generally less than 4 ppm, however, is that the Q_4 peaks are probably all within 1 ppm and likely will affect peak maximum to a limited extent. However, they will be impractical to resolve through curve-fitting as the peaks are likely to be very close. Multiple close peaks may however be the cause of poor fitting of some of the opal-CT samples (see above). Given the results of the present study, we propose that the Q_4 peak position is unlikely to be diagnostic of opal structural type. Injudicious selection of delay time may result in misleading SP spectra, depending on the contribution of the Q_3 component.

Finally, we note that despite the limitations of signal strength, delay time requirements and the need for extensive scans and instrument time, SP is probably the best method to obtain authentic, quantitative ^{29}Si NMR spectra without artificial enhancement of any component.

4.2. T_1 Relaxation

The key findings of the relaxation rate experiments are as follows. First, relaxation rates of opal are variable but are faster than for other forms of silica. Second, relaxation of [29]Si in all forms of opal follows a stretched exponential relationship which can be described by scale (λ) and shape (κ) parameters. Next, there are distinct differences between the scale and shape parameters for opal-AG, opal-AN, opal-CT and other forms of opaline silica. Finally, we note that there may be consistent and discriminatory characteristics of the opal-AG samples from different sources.

While it is difficult to compare simple exponentials to Weibull parameters, we can equate the time taken for say 95% of relaxation to occur. For instance, nacrite, with an exponential relaxation time of 5 h (18,000 s) [60] will reach this level after about 55,000 s. The Q_4 data in Table 1 implies that most of the Australian seam opals will be 95% relaxed after 50 s with some in as short a time as 30 s. The fastest shows a scale factor of 5 s though some samples of opal-AG are significantly slower with figures up to at least 4000 s for the "Spanish menilites". The limited number of Slovakian opals also show slower relaxation. While some examples of opal-AN may be relatively slow (over 10,000 s) all samples studied here appear to relax faster than quartz (see Figure 2 in [59]).

After excitation, nuclei undergo relaxation to return to the ground state. This occurs through two main processes—longitudinal (spin-lattice) and transverse (spin-spin) relaxation processes with time constants designated as T_1 and T_2 respectively. Spin-lattice relaxation processes in solid state NMR occur via dipole-dipole interactions, chemical shift anisotropy, and molecular motion. Dipole-dipole interactions may occur between adjacent spin nuclear spins, or between nuclear spin and hydrogen nuclei, or by interaction with unpaired electrons in paramagnetic species and are governed by a $1/r^6$ dependency.

As [29]Si is only present at 4.7% of the total nuclei then on average only 17.5% of the Si nuclei will be within two atoms of a suitable silicon for a Q_4 centre to relax. In contrast, hydrogen nuclei (as either molecular water or silanol groups) would be expected to be more prevalent within the structure. In addition, paramagnetic centres present as ionic species or molecular oxygen may also be expected to assist in [29]Si relaxation.

Finally, the limited motion in quartz coupled with weak [29]Si-[29]Si dipolar coupling probably accounts for the very slow T_1 times observed. The enhancement to relaxation implies access to spin-lattice relaxation mechanisms in opal that are not available for silica glass or quartz and thus relaxation increases (the scale parameter, λ, is reduced).

The major differences between quartz and opal are as follows. Quartz has a rigid and regular crystal structure exhibiting sharp peaks in XRD patterns suggesting a crystalline structure. In contrast, opal-AG and opal-AN show little obvious regularity with only a single broad peak seen [9]. While the diffraction pattern for opal-CT shows more structure [9], the peaks are still nonetheless broad. There are also chemical differences. Quartz comprises fully silicate bridged O_3Si-O-SiO_3 Q_4 centres whereas all types of opal will include some silanol O_3Si-O-H Q_3 sites and different silicate topologies (see above). Opals also contain varying amounts of so-called "impurities" (Appendix B and Supplementary Materials) including cations replacing Si^{4+} in the matrix (e.g., Al^{3+} accompanied by other cations for charge balance), other metal ions (in undetermined coordination with oxygen) as well as other solutes possibly associated with opal diagenesis. These include group 2a and 2b elements such as Na^+ and Mg^{2+}. While anions are not usually measured, we noted significant amounts of phosphorus in the samples studied here, implying the presence of phosphate. Finally, molecular water may be present, probably with varying ionic strengths due to the presence of solutes. Thus, we propose that the key contributors to enhanced T_1 relaxation are likely to derive from adjacent hydrogens (in water or silanol), paramagnetic metal ions and molecular motion.

To assist investigation of the enhanced relaxation, we present consolidated Q_3 and Q_4 data for scale factors versus shape factor (from Tables 1 and 2) in Figure 4. Apparent is a clear trend from low shape factors and relatively fast relaxation to slower relaxation coupled with higher shape factors. Data is plotted in an alternative form in Figure 5 which compares Q_3 and Q_4 scale and shape terms for individual samples. While there is a possible break point at $\lambda \approx 50$, in general there is an overall trend correlating the Q_3 and Q_4 scale parameters (Figure 5a) with a slope of around 1.4. Figure 5b shows a correlation of Q_3 and Q_4 shape factors with slope of less than unity, though with scatter. Values for Q_4 are generally lower than for Q_3 though are usually within 0.1.

Plotting in these forms, particularly for Figure 4, allows vertical and horizontal comparisons to investigate differences between individual samples to explore the likely impact of the factors noted above, as discussed below. There are also clear zones in both Figures 4a and 5a with, for instance, Australian seam opals at lower left and opal-AN at upper right.
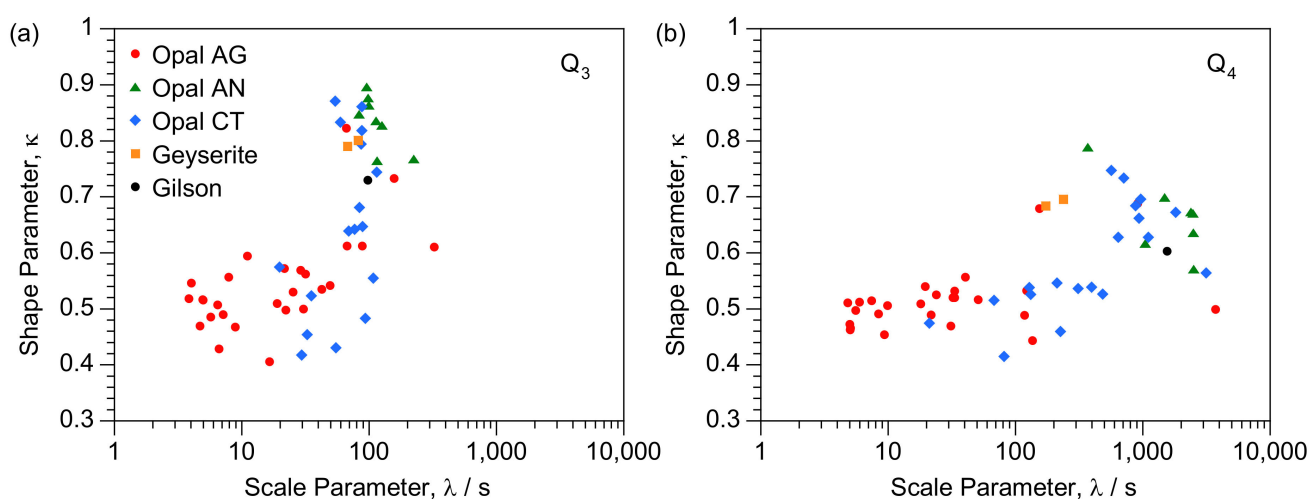
Figure 4. Correlation of consolidated scale and shape parameters for (**a**) Q_3 and (**b**) Q_4 and designated with opal type.
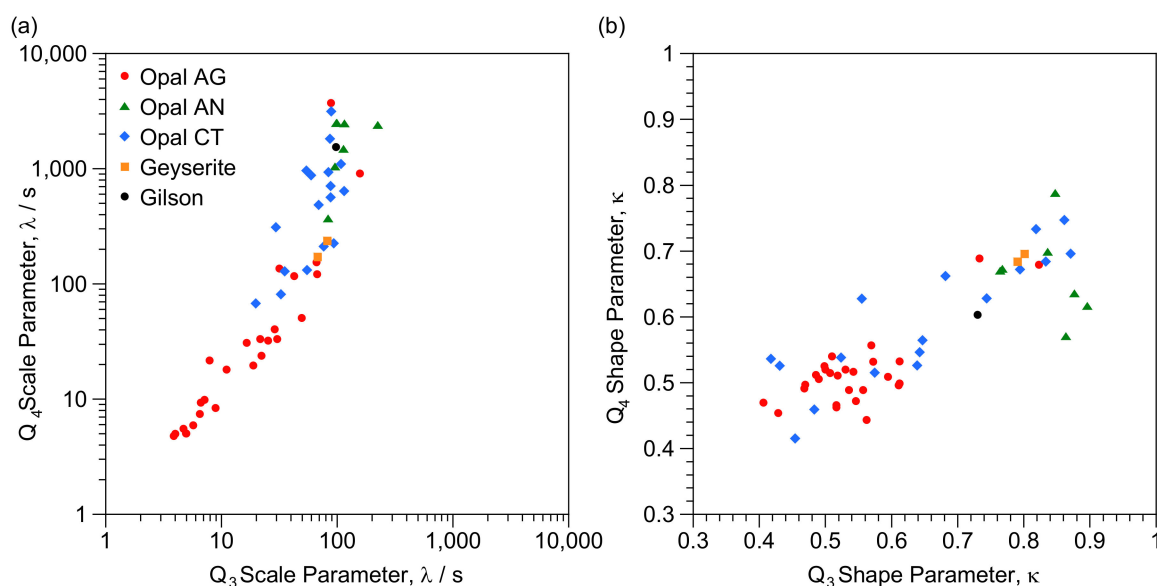
Figure 5. Correlation of scale and shape parameters for (**a**) Q_3 and Q_4 scale parameters (**b**) Q_3 and Q_4 shape parameters and designated with opal type.

First, we examine the influence of "metal ion impurities". In this (see Appendix B and Supplementary Materials) and previous work [12,14,16,20–22,77] it has been demonstrated that many transition metal, f-block and heavy metal elements may be present. We note, however, that there is no compelling case to invoke the presence of such ions to effect relaxation rate enhancement, at least for opal-A. Gilson synthetic opal shows properties similar to opal-A including enhanced relaxation. The Gilson analogue is manufactured by hydrolysis of tetraethoxylsilane and contains no additional metal ions.

A significant difference between opal-AG and opal-AN lies in the much lower concentration of $[Al^{3+}]$ for hyalites, as shown in this work (Appendix B). A wide range of $[Al^{3+}]$ has been reported for gem opals [16,30,78]. Al^{3+} may contribute to spin-diffusion via a ^{29}Si-O-^{27}Al bridge. Enough $^{27}Al^{3+}$ may be present to be detected by NMR in opal-AG and opal-CT [47] and follows tetrahedral geometry suggesting incorporation into the silicate matrix which may also cause structural effects. While opal-AG samples show faster relaxation than opal-AN we note that G32740 (opal-AN from Czechia with 8.1 ppm [Al]) has more Al^{3+} than OOC10 (opal-AN from Lesvos, Greece with 0.46 ppm [Al]) though both share similar Q3 and Q4 parameters.

Next, we examine the enhancement effected by transition metals, for instance Fe^{n+} [71], whose concentration varies from below the detection limit to 1000 ppm for some examples of opal-AG. A value of 17500 ppm was seen for GNEW03 (from Tanzania). This showed a relatively rapid combined Q3 and Q4 scale parameter of 23 s (see above). This high level of $[Fe^{n+}]$ [16,77] has been noted before for Australian seam opals from the Great Artesian Basin (GAB). For instance, the three samples from the dark and black [79] opal site of Lightning Ridge, Australia, all relax very quickly though, possibly contrary to expectation, the opaque blue-grey sample (T2233) relaxes more slowly than two other examples (G13767) which appear as pale yellow and orange glasses. However, G32740 (6.3 ppm) contains more Fe^{n+} than OOC10 (<0.1 ppm) but again shows similar relaxation parameters.

Some samples of opal-AN are fluorescent due to the presence of UO_2^{2+} species [80,81]. OOC10, T18117 (from N. Carolina, USA) and T18511 (Arkaroola, Australia) all contain higher levels of uranium (typically >15 ppm) than the other samples (Appendix B) and while all are among the fastest to relax, they have similar rate for the Q3 component to that for G32740 which contains very little (<1 ppm). The last, however, contains the highest level of $[Fe^{n+}]$ of the samples studied here though and much less than those of the Australian opal-AG samples.

This discussion is, of course, complicated by lack of knowledge of where such ions are located. For instance, it remains to be seen if Fe^{n+} replace Si^{4+} in the opal matrix or if it is randomly located in aqueous residues between zones of silica. No convincing case can be made for an overriding increase in relaxation caused by such ions though minor effects may be expected, though probably difficult to ascribe to any particular element.

Similarly, the presence of molecular oxygen is likely to be a major source of enhancement. The nitrogen flushing experiments (Table 1) of the opal-AG samples of G1401 and G8608 show no obvious major effects with parameters associated with the major Q_4 component being similar. The differences seen for the minor Q_3 peaks probably just reflect a shallow fitting minimum with a trade-off between λ and κ (see above).

The amount and location of hydrogen nuclei in water/silanol is however likely to be the most fruitful source of both enhanced relaxation and differentiation. It has been reported previously [51] that T_1 reduces from 11,000 to 7000 s in going from low to high water content silica glass, though the location of the water was not determined. There are a number of possible sites to provide the necessary hydrogens to effect dipole-dipole interaction. This may occur via adjacent water molecules or through Q_3 centres via $^{29}Si\text{-}O\text{-}^1H$ dipole interactions. Q_3 peaks in MQ silicone co-polymers have faster relaxation rates than for Q_4 due to the proximity of hydroxyl to silicon [82]. The question of the location and level of water in opal is however a difficult topic [10,13,72] though the presence of both silanol and free water has been demonstrated [47,52,58,83]. All samples studied in this study show a complicated ^1H NMR spectrum comprising (to be reported elsewhere) peaks attributable to different water and silanol chemical environments though with differences between opal types. An example is given by the two experiments involving different zones of the hydrophane opal G34475 (Supplementary Materials). Both contain same ratio of Q_3 to Q_4 while differences in water level are probably the cause of the observed dissimilarity under the SEM (see Figure 16 in [41]). As the opaque zone relaxes more slowly, a proposition is that this contains less water, or that it is located farther from the silicon centres.

Finally, we consider molecular motion. This is likely to occur through two mechanisms: local motion relating to the silica tetrahedra, akin to rotations, and vibrations and generic translational thermal mobility. The latter may be enhanced by the physical effect of spinning in the NMR probe which may be enhanced by friction-based heating. Given that opal-AG and opal-AN have the same XRD patterns then the bulk structures are unlikely to be the source of any differences in molecular motion. Nevertheless, we expect that "lattice" motion will be different for each opal type though definitive evidence is lacking.

The most striking observation in the current work is the difference in shape parameter, particularly between opal-AG and opal-AN. The literature, however, is sparse with only limited data available for the "spin-dilute" ^{29}Si system. The dominance of CP studies has also rendered this as a neglected area for opal. A shape parameter of less than 1, has been reported before for ^{29}Si NMR with values in the range 0.5 to 1 for silicon carbide [61] and a figure of 0.5 for a volcano derived silica coating [48]. One study of silica glass gave a better fit with a shape factor of 0.9 rather than as an exponential [54] ($\kappa = 1$). It has been proposed that a shape factor of 0.5 is due to relaxation via random (three dimensional) distribution of paramagnetic centres [48] with no contribution from spin-diffusion [63], based on earlier theoretical studies [84,85]. Values of 0.5–1.0 have, however, been described and may be due to non-random distribution of paramagnetic centres [48,61], partial contribution of spin-diffusion [63,86] or degree of glassiness [87].

We hypothesize that the major differences in scale and shape factor between, for instance, opal-AG and opal-AN are mostly due to the amount and distribution of water/silanol and to a lesser extent other metal ions. Shape factor values of 0.5 will occur where there is an even and uniform distribution causing a three-dimensional arrangement with equal probabilities of encountering paramagnetic centres in all directions. Higher shape factors values would arise if there is localization of water, silanol or the "impurity" metal ions. For instance, water may be collected as micro-inclusions. Similarly, Q_3 silanols may be grouped (rather than uniformly distributed) and associated with hydrogen-bonded

water, which may contain metal ions as solutes. Consistent with this is the observation that the largest values for κ occur for Q_3 (Figure 4) while the spread of values suggest greater variability for these sites in comparison with Q_4. Q_2 (gem-silanol) may be present and while there is little evidence for substantial amounts in the present work (peak in the range -90 to -95 ppm) [46] their effect, if present, may be considerably more than Q_3 and Q_4. Q_4 sites are likely to be remote from such centres and are thus more subject to a general bulk effect. In contrast, it is likely that the amount, rather than the distribution, of these paramagnetic centres that influences the scale factor. Those samples that show very slow Q_4 relaxation are presumably very remote from the water and metal ion sites. Compounded with the $1/r^6$ law, this is likely to be a very variable feature, as observed for opal-AN.

4.3. Implications for the Formation and Characterisation of Opal-A

Opal-AG and opal-AN show clear differences both in the SP spectrum and in the T_1 relaxation parameters (Table 1). This is possibly to be expected as the two have very distinct microstructures when viewed by SEM and from what is known about the conditions of formation. What is surprising, however, is the magnitude of the differences, particularly when compared with the minor differences seen in the Raman and IR spectra [41].

Chemical aspects of the formation of silica in general [88] and particularly precious opal-AG have been a topic of interest for many years though as yet only a generic mechanism may be proposed [20,32,34,67,89,90]. Irrespective of the source of water, or the nature of the host rock, it is proposed that a saturated (or near saturated) silicic acid solution is generated by aqueous action on silicate rich rocks [20,32,34,67,89,90]. This liquor is sequestrated in gaps in weathered terrain and slowly forms the necessary silica spheres to effect Bragg diffraction in POC opal. Optimum conditions for POC creation, such as temperature, pH, other metal species, ionic strength and the presence of nucleating centres are open to conjecture though a reasonable proposition is that formation should be slow allowing consistent geometries of similarly sized spheres to deposit. It is probable that slow deposition from a colloidal suspension of variable viscosity results in a uniform three-dimensional arrangement. This would be consistent with the relatively fast relaxation seen for the opal-AG samples and shape factors of about 0.5. Indeed, these seem typical for the seam opal associated with sedimentary rocks covering the southern Bulldog Shale region of the GAB (from South Australia and New South Wales) [90] comprising the current and recent Australian mining centres of Andamooka, Coober Pedy, Lambina, Lightning Ridge, Mintabie and White Cliffs.

Examination of the data in Table 1 suggests that T_1 relaxation may provide insights into the formation conditions, or at least correlate with conditions of deposition, for instance affecting the speed of deposition. The two examples of Winton-formation boulder opal also show slower T_1 relaxation, which might be linked to formation in ironstone rather than kaolin or clay as in the other major opal fields in Australia. The shape parameters are also slightly higher than for the Australian seam opals though the sample size is small. Fossilized Cretaceous (Aptian) molluscs (probably *Eyrena* and *Peratobelus*) from Coober Pedy show slower relaxation and, interestingly, similar Q_3 and Q_4 parameters which might be a consequence of replacement of calcite or aragonite and a distinct different formation process to that for seam opals.

The Slovakian samples probably formed under a pressure/temperature condition similar to those of the Australian seam opals, but in different rock types [28] and have slightly slower T_1 relaxation values. Figure 6 (G34280 from Cerenvenica in Slovakia) shows zones both of regular lines of spheres and irregular arrays similar to that seen for other samples from these sites [28] and for a hydrophane (G34475) [41]. G34280 itself shows extreme values for the Q_3 to Q_4 ratio and the highest shape factor values, though all over indications are that it should be classified as opal-AG. It is possible that the high level of Q_3 effects major structural change. The example of a hydrophane also shows complex SEM images [41] and while the optically distinct zones show different scale factors, both the

shape factors and the calculated (infinite time) Q_3 to Q_4 ratios are the same (Supplementary Materials). This would be consistent with the reversible ability to take up water and thus provide the necessary adjacent hydrogen nuclei (faster relaxation) without any chemical change to the silica matrix itself.
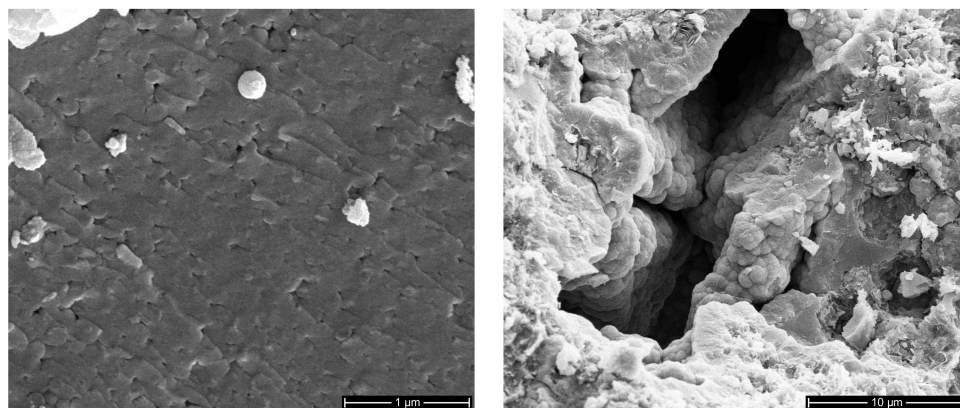
Figure 6. SEM images of freshly ground G34280 (opal-AG from Cerenvenica, Slovakia) showing mixed zones.

The examples of the chert-based "Spanish menilites" are again distinct with slow Q_3 and very slow Q_4 T_1 relaxation. SEM images [41,66] also show irregular assemblages of silica spheres. A biogenic-derived formation mechanism involving diatomite has been proposed [66]. Very different relaxation characteristics are thus not surprising as they may not be "typical" examples of opal-AG as from Australia or Slovakia. The slightly higher κ values for the Q_3 centres may imply a marginally different silanol environment to for instance seam opals. In contrast, an opal-CT specimen from the same site (GNEW09) shows parameters which seem more typical for the type with a Q_4 scale parameter of 566 s. The Q_3 to Q_4 ratio of 0.13, however, was similar to the 0.15 found for GNEW01 (Table 1). The very high shape for parameter for GNEW09 (0.86) for Q_3 also suggests similar origins as has been suggested for this site [66].

Opal-AN, on the other hand, forms at higher temperature by vapor deposition [31] and has undergone significantly rapid cooling and thus potential fractionation of water/silanol, possibly with formation of aqueous micro-inclusions and formation of pockets of high Q_3 density. The lower ratio of Q_3 to Q_4 in opal-AN when compared with opal-AG is demonstrated by the extrapolation of the final peak areas.

The two samples of geyserite show a shape factor of 0.7 which would be consistent with the higher formation temperature [12], while the NMR spectra are more like those for opal-AN rather than opal-AG.

Data for the Gilson synthetic opal is also enlightening. We have demonstrated a characteristic set of parameters such as low Q_3 to Q_4 ratio and a very slow Q_4 relaxation, at least for the sample studied. The relatively fast relaxation of Q_3 implies the presence of accessible water in the matrix while the high shape factor implies clusters of incomplete hydrolysis. T_1 relaxation potentially provides ready differentiation from Australian seam opals.

We also note a continuing problem with the term "opal". While opal-A, opal-CT and opal-C are accepted overarching terms, this may be misleading since it implies some sort of similarity between the various forms. XRD analysis provides a delineating structural, rather than paragenetic classification, for instance of opal-A. This is, of course, well known for opal-AN through major differences under the SEM. The NMR results in this work provide further support for structural differentiation. Thus, hyalite may prove to be a better term rather than opal-AN, even noting spectroscopic similarities through some techniques with opal-AG. The remaining types of opal-A (Table 1) show common features such as the presence of silica spheres though in our experience we find these show differing levels of regularity (see this paper and previous images of unetched samples [9,41]). The T_1

relaxation features may thus provide a further delineation. We suggest that any examination of new sources of material, or a re-interpretation of old sites, should include a ^{29}Si SP NMR spectrum and a T_1 relaxation experiment to build up a corpus of reference material. For instance, other examples of authenticated "white or milky opals" [16] from sites such as Honduras [16,91], Brazil [16], Mexico [28], Madagascar [8] and the USA [33] may prove to have distinct characteristics.

T_1 studies may also provide evidence of provenance. For instance, in this work the Australian seam opals showed distinctively faster relaxation when compared to those from other Australian sites, such as Queensland boulder opals and opalised fossils. Further work will be required to see if trends appear between the different regions (e.g., Coober Pedy versus Lightning Ridge) and within localities (e.g., the different fields at Coober Pedy). Examination of POC types, such as "pinfire" or "harlequin" may also provide insights. It is noted that only about 100 mg of sample is required for this testing, though the measurement is effectively "destructive". Any observed trends may provide insights into formation conditions and possible dating of the deposits. This may assist in further exploration. Finally, we note the distinctive results of the opalised fossils which merits further and directed study covering other organisms (e.g., marine reptiles) and sites (e.g., comparison of Coober Pedy and Lightning Ridge).

4.4. Implications for Characterisation of Opal-CT

Opal-CT spectra and relaxation properties are similar in nature to those for opal-AG and opal-AN with all showing peaks that can be assigned to Q_3 and Q_4. A major difference shown by ^{29}Si SP NMR is that, in general, opal-CT samples show lower proportions of Q_3 than opal-AG as judged by the presumed Q_3 peak at around -104 ppm. In addition, shape and scale parameters span a larger range. Several features may be exploited from this study, as follows.

First, we examine the "boundary" between opal-AG and opal-CT. This notion is supported by transitional XRD forms [9] which show a narrower (than for opal-AG) major XRD pattern peak as well as a small peak at about 2.5 Å for all samples of opal-CT. This trend continues as XRD patterns of opal-CT can be arranged according to increasing structure in the XRD patterns (see Figure 5 in [9]) with clear differentiation of the peak at 4.1 and 4.3 Å [9]. Figures 4 and 5 might be interpreted to suggest a continuum of shape and scale parameters linking opal-AG and opal-CT. However, the trends are misleading as a further implication would be that opal-CT bridges the gap between opal-AG and opal-AN, though consideration of what is known about formation conditions make this untenable. However, both Q_3 to Q_4 ratios (Tables 1 and 2) and the visible appearance of the spectra (Figures 1b and 3) show more similarities of opal-CT to opal-AN than to opal-AG.

Figure 7a shows four representative XRD patterns spanning the proposed boundary with corresponding ^{29}Si NMR spectra in Figure 7b. Little attention should be paid to the major peak positions in the NMR spectra as they are for a fixed delay time with variable contribution from Q_3 and Q_4. The lower (G1442) and upper (GNEW24) plots show NMR spectra typical for opal-AG and opal-CT respectively. The transitional form (orange plot, G14581) can be fitted to respective scale and shape parameters of 10.5 ± 0.1 s/0.52 ± 0.01 (Q_3) and 22.6 ± 0.1 s/0.47 ± 0.01 (Q_4) with an extrapolated Q_3 to Q_4 ratio of 0.26. This is typical for Australian seam opal and may be expected as the sample originates in Andamooka, South Australia and has POC. NMNH Eth S2 (green plot, from Ethiopia), however, appears anomalous with the NMR spectrum showing significant amounts of Q_3 resulting in an asymmetric main peak more like opal-AG than opal-CT. The XRD pattern, however, clearly defines this as opal-CT with the peak at 2.5 Å.

As discussed above, we were also unable to determine discrete Q_3 fitting data for two other samples of opal-CT (GNEW05 and GNEW27), both with relatively simple XRD patterns (as for NMNH Eth S2). Our interpretation is that the "boundary" between opal-AG and opal-CT is not well defined by NMR and, indeed, may vary according to the measurement type. It is perhaps not surprising that the fitting regimes for opal-AG and opal-

CT may not apply in some cases. It is also possible that a re-interpretation of the assignment of the ^{29}Si NMR peaks may be warranted through additional NMR techniques. This is a critical "region" as many POC opal-CT samples show a relatively simple XRD pattern.

(a)   (b)
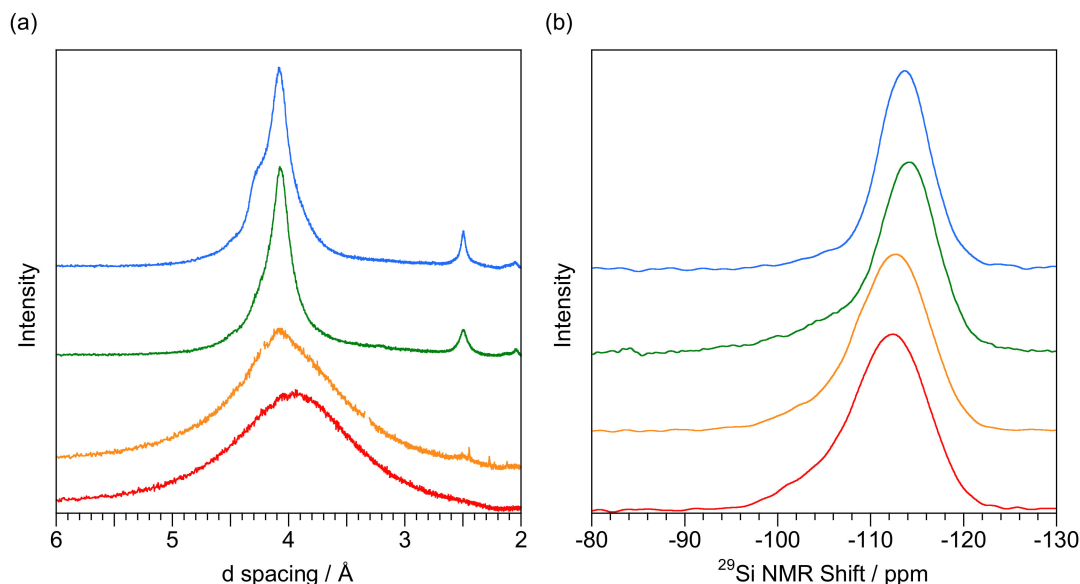
Figure 7. Comparison of opals at the presumed AG to CT boundary (**a**) XRD patterns (**b**) 400 s delay time ^{29}Si SP NMR spectrum for G1401 (opal-AG from White Cliffs NSW, with POC, red), G14581 (opal-AG to opal-CT transitional form from Andamooka, South Australia, orange), NMNH Eth S2 (opal-CT from Mezezo, Ethiopia with POC, green), GNEW24 (opal-CT from Kutahuya, Turkey with no POC, blue). Units are Å (XRD) and ppm (NMR). Major quartz peaks have been deleted from the XRD pattern of G14581.

Next, we examine potential trends across the opal-CT range which might result from the proposed transition (diagenesis) from of opal-A to quartz and moganite [12,34–40]. In previous work [9] we showed correlations between features associated with the four constituent major peaks at 4.3, 4.1, 3.9 and 2.5 Å in the XRD patterns. In one case a relation was noted between the relative area ratios of the 4.3 and 3.9 Å peaks and in the other between the FWHM for the 4.3 and 2.5 Å peaks. There is also a trend to sharper Raman spectroscopy peaks [9]. As noted in Figure 4 there is a loose correlation resulting in a trend from a low (i.e., faster relaxation) scale parameter/low shape factor to higher (i.e., slower relaxation) scale parameter/higher shape factor. It is tempting to ascribe this to a progressive migration of uniform but relatively unstructured Q_3 and Q_4 silica species to more structured forms with fractionation of the components, for instance, with increased ratios of tridymite to cristobalite [35]. In this, water might be expelled resulting in remoteness from the silicon nuclei (higher scale factors) and localized, resulting in higher shape factors owing to uneven distribution. Similarly, dehydration may occur for proximal silanol groups. While both effects may be in operation, we find no convincing support through correlation of any of the NMR parameters with the XRD pattern trends, such as high shape parameters (G32925 and GNEW09). Possibly other features, such as the presence of transition metals obscure any effects. As for other measurement techniques we find no evidence for the complicated NMR spectrum of tridymite [50]. Similar comments may be made about the Q_3 to Q_4 ratios. The highest Q_3 ratios (Table 2) occur for G32925, GNEW09, GNEW30 and T4051. While G32925 and GNEW30 show well defined and separated peaks at 4.1 and 4.3 Å, the peaks at 4.3 Å are less prominent for the other two.

Finally, we reiterate concerns with the naming convention of opal. We have included results both for opal-A and opal-CT for comparison purposes in this paper and while there are clear similarities, there is little homogeneity across the opal range. However,

commercial reasons may dominate structural classification as POC occurs with both opal-AG and opal-CT. Nevertheless, as for opal-A, we propose new work should include the full range of NMR parameters, particularly for those opal-CT samples showing POC.

5. Conclusions

Scale and shape parameters derived from solid-state ^{29}Si SP NMR have proven to be an additional characterisation method for opal providing insights not available by XRD patterns, and Raman and IR spectroscopy. We speculate that ^{29}Si NMR occupies a key position between the between bond length (Raman and IR) and microscopic (or interatomic) (XRD and SEM) scales, probably due to the 3-dimensional lay-out of water and Q_3 species, and short-range structural changes induced by silanol and the conformation of the SiO_4 frameworks. To exploit this further we intend to extend the study to other opal samples as described above, explore the characteristics of hydrogen to silicon magnetization transfer in CP mode and to examine the nature of silanol and water components through ^{1}H NMR.

Appendix A

Table A1. Sample Data: As Labelled on Specimens.

Reference	Type	Location (Australia Unless Noted)	Description
E1937	AN	Mt Cora, New South Wales	colorless glass
G1401	AG	White Cliffs, New South Wales	translucent
G1421	CT	Mt Cora, New South Wales	shiny black
G1442	AG	William Creek, South Australia	glassy white with POC
G7107	AN	Valeč, Czechia	colorless glass
G8608	AG	White Cliffs, New South Wales	opaque white, POC
E1937	AN	Mt Cora, New South Wales	colorless glass
G1401	AG	White Cliffs, New South Wales	translucent
G1421	CT	Mt Cora, New South Wales	shiny black
G1442	AG	William Creek, South Australia	glassy white with POC
G7107	AN	Valeč, Czechia	colorless glass

Table A1. *Cont.*

Reference	Type	Location (Australia Unless Noted)	Description
G8608	AG	White Cliffs, New South Wales	opaque white, POC
G8736	AN	Springsure, Queensland	colorless glass
G8877	AN	Squaretop near Dalby, Queensland	colorless glass
G9258	AG	Andamooka, South Australia	translucent white POC
G7532	AG	Queensland	white with POC on matrix
G7682	AG	Mintabie, South Australia	glassy blue-grey
G9592	AG	Cloncurry, Queensland	milky white with POC
G9811	AG	Coober Pedy, South Australia	opaque white with POC
G9942	CT	Angaston, South Australia	translucent glossy white
G13755	CT	Ross, Tasmania	translucent white
G13761	CT	Marvell Loch, Western Australia	translucent green
G13764	AN	Dalby, Queensland	colorless glass
G13767 [a]	AG	Lightning Ridge, New South Wales, Australia	mixed samples
G14581	AG-CT	Andamooka, South Australia	opaque brown with POC
G21471	A	Rotorua, New Zealand	crumbly white
G32740	AN	Valeč, Czechia	colorless glass
G32925	CT	Zelinograd, Qazaqstan	glassy vermilion
G34475 [b]	AG	Dubnik, Slovakia	white opaque/translucent
G34996 [a]	AG	Coober Pedy, South Australia, Australia	opalised mussels
G34997 [a]	AG	Coober Pedy, South Australia, Australia	opalised belemnites
GNEW01	AG	Caldes de Malavella, Catalonia, Spain	opaque cream
GNEW03	CT	Mt Iyobo, Tanzania	opaque green
GNEW05	CT	Bemia, Madagascar	transparent yellow
GNEW08	CT	Ethiopia	glassy green and brown
GNEW09	CT	Caldes de Malavella, Catalonia, Spain	translucent brown
GNEW19	CT	Tanzania	orange glass
GNEW20	CT	California, USA	translucent yellow
GNEW22	AG	Lambina, South Australia	opaque white with POC
GNEW23	AG	Caldes de Malavella, Catalonia, Spain	opaque grey-brown
GNEW24	CT	Kutahuya, Turkey	translucent olive
GNEW27	CT	Yozgat, Turkey	blue-green glass
GNEW28	CT	Yozgat, Turkey	olive-green glass
GNEW30	CT	East of Manzano Mts, New Mexico, USA	opaque white
GNEW31	AG	Andamooka, South Australia, Australia	translucent white
M8736	AN	Springsure, Queensland	colorless glass
M53441	CT	Kremze, Czechia	opaque blue
MS-4	AN	Mt Squaretop, Queensland	colorless glass
NMNH ETH S2	CT	Mezezo, Ethiopia	brown bottle glass, POC
OOC3	CT	Ménilmontant, France	opaque grey-brown
OOC5	CT	Virgin Valley, Nevada, USA	opaque white
OOC10	AN	Lesvos, Greece	colorless glass
SO3	AG	Dubnik, Slovakia	translucent with POC
SO7	AG	Dubnik, Slovakia	opaque white
SO17	AG	Dubnik, Slovakia	opaque white
T1665	A	Rotorua, New Zealand	crumbly white
T2233	AG	Lightning Ridge, New South Wales	blue-grey glass
T4051	CT	Charlies Swamp, South Australia	translucent grey
T18117	AN	Mitchell Co. N. Carolina, USA	colorless glass
T18511	AN	Mt Gee, Arkaroola, South Australia	colorless glass
T22842	CT	Missoula, Montana, USA	opaque white
WBO1	AG	Winton, Queensland, Australia	bluish opaque, POC

[a] Collection of samples from the same location. [b] different zones of the same piece used.

Appendix B

Table A2. Selected Elemental Analyses (ppm by Weight) (see Supplementary Materials for Full Table).

		^{27}Al	^{31}P	^{49}Ti	^{51}V	^{55}Mn	^{57}Fe	^{59}Co	^{60}Ni	^{65}Cu	^{137}Ba	^{238}U
Opal-AG												
	G1401	6580	3.12	6.83	0.0701	9.17	485	0.0109	0.0694	0.0288	155	0.0265
	G9811	5990	3.54	5.30	0.0896	5.50	393	0.0139	0.0566	0.0267	154	0.0265
	T2233	6110	39.1	722	4.76	18.5	1040	50.0	17.3	159	144	2.36
	G8608	4560	3.53	8.36	0.0895	5.30	271	0.0553	0.100	0.146	83.8	0.0572

Table A2. *Cont.*

		^{27}Al	^{31}P	^{49}Ti	^{51}V	^{55}Mn	^{57}Fe	^{59}Co	^{60}Ni	^{65}Cu	^{137}Ba	^{238}U
Opal-AN												
	E1937	5.19	3.29	0.128	0.347	0.0261	0.220	3.61×10^{-3}	0.0236	9.03×10^{-3}	0.122	0.298
	MS-4	6.42	3.55	0.0207	0.495	0.0322	— [a]	— [a]	3.55×10^{-3}	— [a]	2.27×10^{-4}	0.135
	G32740	8.10	8.43	0.633	0.458	0.122	6.30	0.0274	0.159	0.547	0.181	0.034
	M8736	3.57	3.33	9.34×10^{-3}	0.434	0.024	— [a]	— [a]	0.0192	7.57×10^{-3}	4.38×10^{-3}	0.116
	OOC10	0.458	3.30	6.02×10^{-3}	0.233	0.0247	— [a]	8.83×10^{-4}	0.0217	0.0224	0.139	15.2
	T18511	0.893	3.34	0.0109	0.0417	0.0272	— [a]	— [a]	3.43×10^{-3}	2.43×10^{-3}	0.0127	24.9
	T18117	16.0	5.11	0.214	0.015	7.14	4.11	0.0260	0.0705	2.49	0.985	54.8
	G7107	22.6	4.78	0.352	0.578	0.0526	2.31	7.50×10^{-4}	0.0221	0.0376	0.0257	0.053
	G8877	0.273	3.35	0.0654	0.775	0.0259	— [a]	1.77×10^{-3}	0.0186	0.0277	0.0251	0.381
	G13764	3.13	3.16	0.0403	0.0466	0.0328	— [a]	— [a]	0.0200	0.0281	2.44×10^{-3}	0.295
Opal-CT												
	G9942	29.8	3.93	2.70	0.348	0.267	54.3	0.0238	0.0951	0.124	0.06	0.0874
	ETH S2	6760	2.86	46.8	5.36×10^{-4}	17.1	724	0.0184	0.0226	0.0208	25.6	0.781
	GNEW03	3640	4.30	0.330	0.804	2.43	17,500	1.14	9.62	8.85	1.96	0.212
	OOC3	4320	16.6	743	57.4	1.51	1100	0.649	7.23	8.28	6.04	0.346
	T22842	0.371	5.84	0.0829	0.224	0.137	201	4.22×10^{-3}	0.0748	3.06	0.996	21.7

[a] Very low concentration.

References

1. Jones, J.B.; Sanders, J.V.; Segnit, E.R. Structure of opal. *Nature* **1964**, *204*, 990–991. [CrossRef]
2. Jones, J.B.; Segnit, E.R. The Nature of Opal I. Nomenclature and Constituent Phases. *J. Geol. Soc. Aust.* **1971**, *18*, 57–68. [CrossRef]
3. Smith, D.K. Opal, cristobalite and tridymite: Noncrystallinity versus crystallinity, nomenclature of the silica minerals and bibliography. *Powder Diffr.* **1998**, *13*, 2–19. [CrossRef]
4. Elzea, J.M.; Rice, S.B. TEM and X-Ray diffraction evidence for cristobalite and tridymite stacking sequences in opal. *Clays Clay Miner.* **1996**, *44*, 492–500. [CrossRef]
5. Ghisoli, C.; Caucia, F.; Marinoni, L. XRPD patterns of opals: A brief review and new results from recent studies. *Powder Diffr.* **2010**, *25*, 274–282. [CrossRef]
6. Caucia, F.; Marinoni, L.; Bordini, V.; Ghisoli, C.; Adamo, I. Physical and chemical properties of some Italian opals. *Period. Mineral.* **2012**, *81*, 93–106.
7. Eckert, J.; Gourdon, O.; Jacob, D.E.; Meral, C.; Monteiro, P.J.M.; Vogel, S.C.; Wirth, R.; Wenk, H.-R. Ordering of water in opals with different microstructures. *Eur. J. Mineral.* **2015**, *27*, 203–213. [CrossRef]
8. Sodo, A.; Municchia, A.C.; Barucca, S.; Bellatreccia, F.; Ventura, G.D.; Butini, F.; Ricci, M.A. Raman, FT-IR and XRD investigation of natural opals. *J. Raman Spectrosc.* **2016**, *47*, 1444–1451. [CrossRef]
9. Curtis, N.J.; Gascooke, J.R.; Johnston, M.R.; Pring, A. A Review of the Classification of Opals with Reference to Recent New Localities. *Minerals* **2019**, *9*, 299. [CrossRef]
10. Segnit, E.R.; Stevens, T.J.; Jones, J.B. The Role of Water in Opals. *J. Geol. Soc. Aust.* **1965**, *12*, 211–226. [CrossRef]
11. Sosnowska, I.; Buchenau, U.; Reichenauer, G.; Graetsch, H.; Ibel, K.; Frick, B. Structure and dynamics of the opal-water system. *Phys. B* **1997**, *234*, 455–457. [CrossRef]
12. Jones, B. Siliceous sinters in thermal spring systems: Review of their mineralogy, diagenesis, and fabrics. *Sediment. Geol.* **2021**, *413*, 105820. [CrossRef]
13. Day, R.; Jones, B. Variations in water content in opal-A and opal-CT from geyser discharge aprons. *J. Sediment. Res.* **2008**, *78*, 301–315. [CrossRef]
14. McOrist, G.D.; Smallwood, A. Trace elements in precious and common opals using neutron activation analysis. *J. Radioanal. Nucl. Chem.* **1997**, *223*, 9–15. [CrossRef]
15. Thomas, P.S.; Brown, L.D.; Ray, A.S.; Prince, K.E. A SIMS study of the transition elemental distribution beyween bands in banded sedimentary opal from the Lightning Ridge locality. *Neues Jahrb. Minerol. Abh.* **2006**, *182*, 193–999.
16. Gaillou, E.; Delaunay, A.; Rondeau, B.; Bouhnik-le-Coz, M.; Fritsch, E.; Corren, G.; Monnier, C. The geochemistry of gem opals as evidence of their origin. *Ore Geol. Rev.* **2008**, *34*, 113–126. [CrossRef]
17. Ansori, C. Model mineralisasi pembentukan opal banten. *J. Geol. Indones.* **2010**, *5*, 151–170. [CrossRef]
18. Simoni, M.; Caucia, F.; Adamo, I.; Galinetto, P. New occurence of fire opal from Bemia, Madagascar. *Gems Gemol.* **2010**, *46*, 114–121. [CrossRef]
19. Rondeau, B.; Cenki-Tok, B.; Fritsch, E.; Mazzero, F.; Gauthier, J.-P.; Bodeur, Y.; Bekele, E.; Gaillou, E.; Ayalew, D. Geochemical and petrological characterizarion of gem opals from Wegel Tena, Wolo, Ethiopia: Opal formation in an Oligocene soil. *Geochem. Explan. Environ. Anal.* **2012**, *12*, 93–104. [CrossRef]
20. Liesegang, M.; Milke, R. Australian sedimentary opal-A and its associated minerals: Implications for natural silica sphere formation. *Am. Mineral.* **2014**, *99*, 1488–1499. [CrossRef]
21. Dutkiewicz, A.; Landgrebe, T.C.W.; Rey, P.F. Origin of silica and fingerprinting of Australian sedimentary opals. *Gondwana Res.* **2015**, *27*, 786–795. [CrossRef]

22. McOrist, G.D.; Smallwood, A.; Fardy, J.J. Trace elements in Australian opals using neutron activation analysis. *J. Radioanal. Nucl. Chem. Artic.* **1994**, *185*, 293–303. [CrossRef]

23. Bobon, M.; Christy, A.A.; Kluvanec, D.; Illasova, L. State of water molecules and silanol groups in opal minerals: A near infrared spectrscopic study of opals from Slovakia. *Phys. Chem. Miner.* **2011**, *38*, 809–818. [CrossRef]

24. Chauviré, B.; Rondeau, B.; Mangold, N. Near infrared signature of opal and chalcedony as a proxy for their structure and formation conditions. *Eur. J. Mineral.* **2017**, *29*, 409–421. [CrossRef]

25. Pineau, M.; Deit, L.L.; Chauviré, B.; Carter, J.; Rondeau, B.; Mangold, N. Toward the geological significance of hydrated silica detected by near infrared spectroscopy on Mars based on terrestrial reference samples. *Icarus* **2020**, *348*, 113706. [CrossRef]

26. Wilson, M.J. The structure of opal-CT revisited. *J. Non-Cryst. Solids* **2014**, *405*, 68–75. [CrossRef]

27. Fröhlich, F. The opal-CT nanostructure. *J. Non-Cryst. Solids* **2020**, *533*, 119938. [CrossRef]

28. Rondeau, B.; Fritz, E.; Guiraud, M.; Renac, C. Opals from Slovakia ("Hungarian opals"): A reassesment of the conditions of formation. *Eur. J. Mineral.* **2004**, *16*, 789–799. [CrossRef]

29. Spencer, R.J.; Levinson, A.A.; Koivula, J.L. Opals from Querétaro Mexico: Fluid inclusion study. *Gems Gemmol.* **1992**, *28*, 28–34. [CrossRef]

30. Chauviré, B.; Rondeau, B.; Alexandre, A.; Chamard-Boris, S.; La, C.; Mazzero, F. Pedogenic origin of precious opals from Wegel Tena (Ethiopia): Evidence from trace elements and oxygen isotopes. *Appl. Geochem.* **2019**, *101*, 127–139. [CrossRef]

31. Floerke, O.W.; Jones, J.B.; Segnit, E.R. The genesis of hyalite. *Neues Jahrb. Mineral. Mon.* **1973**, *2*, 82–89. [CrossRef]

32. Jones, J.B.; Segnit, E.R. The Occurence and Formation of Opal at Coober Pedy and Andamooka. *Aust. J. Sci.* **1966**, *29*, 129–133.

33. Martin, E.; Gaillou, E. Insight on gem opal formation in volcanic ash deposits from a supereruption: A case study through oxygen and hydrogen isotopic composition of opals from Lake Tecopa, California, USA. *Am. Mineral.* **2018**, *103*, 803–811. [CrossRef]

34. Williams, L.A.; Crerar, D.A. Silica diagenesis, II. General mechanisms. *J. Sediment. Petrol.* **1985**, *55*, 312–321.

35. Liesegang, M.; Tomaschek, F. Tracing the continental diagenetic loop of the opal-A to opal-CT transformation with X-ray diffraction. *Sediment. Geol.* **2020**, *398*, 105603. [CrossRef]

36. Lynne, B.Y.; Campbell, K.A.; Moore, J.N.; Browne, P.R.L. Diagenesis of 1900-year-old siliceous sinter (opal-A to quartz) at Opal Mound, Roosevelt Hot Springs, Utah, U.S.A. *Sediment. Geol.* **2005**, *179*, 249–278. [CrossRef]

37. Kano, K. Ordering of opal-CT in diagenesis. *Geochem. J.* **1983**, *17*, 87–93. [CrossRef]

38. Rice, S.B.; Freund, H.; Huang, W.-L.; Clouse, J.A.; Isaacs, C.M. Application of Fourier transform infrared spectroscopy to silica diagenis: The opal-A to opal-CT transformation. *J. Sediment. Res.* **1995**, *A65*, 639–647.

39. Herdianita, N.R.; Browne, P.R.L.; Rodgers, K.A.; Campbell, K.A. Mineralogical and textural changes accompanying ageing of silica sinter. *Miner. Depos.* **2000**, *35*, 48–62. [CrossRef]

40. Jones, B.; Renaut, R.W. Microstructural changes accompanying the opal-A to opal-CT transition: New evidence from the siliceous sinters of Geysir, Haukadalur, Iceland. *Sedimentology* **2007**, *54*, 921–948. [CrossRef]

41. Curtis, N.J.; Gascooke, J.R.; Pring, A. Silicon-oxygen region infra-red and Raman analysis of opals: The effect of sample preparation and measurement type. *Minerals* **2021**, *11*, 173. [CrossRef]

42. de Jong, B.W.H.S.; van Hoek, J.; Veeeman, W.S.; Manson, D.V. X-ray diffraction and ^{29}Si magic-angle-spinning NMR of opals: Incoherent long- and short-range order in opal-CT. *Am. Mineral.* **1987**, *72*, 1195–1203.

43. Graetsch, H.; Mosset, A.; Gies, H. XRD and ^{29}Si MAS-NMR study of some non-crystalline silica minerals. *J. Non-Cryst. Solids* **1990**, *119*, 173–190. [CrossRef]

44. Adams, S.J.; Hawkes, G.E.; Curzon, E.H. A solid state ^{29}Si nuclear magnetic resonance study of opal and other hydrous silicas. *Am. Mineral.* **1991**, *76*, 186371.

45. Graetsch, H.; Gies, H.; Topalovic, I. NMR, XRD and IR study on microcrstalline opal. *Phys. Chem. Miner.* **1994**, *21*, 166–175. [CrossRef]

46. Brown, L.D.; Ray, A.S.; Thomas, P.S. ^{29}Si and ^{27}Al NMR study of amorphous and paracrystalline opals from Australia. *J. Non-Cryst. Solids* **2003**, *332*, 242–248. [CrossRef]

47. Paris, M.; Fritsch, E.; Aguilar-Reyes, B. ^{1}H, ^{29}Si and ^{27}Al NMR study of the destabilization process of a paracrystalline opal from Mexico. *J. Non-Cryst. Solids* **2007**, *353*, 1650–1656. [CrossRef]

48. Chemtob, S.M.; Rossman, G.R.; Stebbins, J.F. Natural hydrous amorphous silica: Quantitation of network speciation and hydroxyl content by ^{29}Si MAS NMR and vibrational spectroscopy. *Am. Mineral.* **2012**, *97*, 203–211. [CrossRef]

49. Lippmaa, E.; Mági, M.; Samoson, A.; Engelhard, G.; Grimmer, A.-R. Structural Studies of Silicates by Solid-State High-Resolution ^{29}Si NMR. *J. Am. Chem. Soc.* **1980**, *102*, 4889–4893. [CrossRef]

50. Smith, J.V.; Blackwell, C.S. Nuclear magnetic resonance of silica polymorphs. *Nature* **1983**, *303*, 223–225. [CrossRef]

51. Gladden, L.F.; Carpenter, T.A.; Elliot, S.R. ^{29}Si MAS NMR studies of the spin-lattice relaxation time and bond-angle distribution in vitreous silica. *Philos. Mag. B* **1986**, *53*, L81–L87. [CrossRef]

52. Liu, C.C.; Maciel, G.E. The Fumed Silica Surface: A Study by NMR. *J. Am. Chem. Soc.* **1996**, *118*, 5103–5119. [CrossRef]

53. Léonardelli, S.; Facchini, L.; Fretigny, C.; Tougne, P.; Legrand, A.P. Silicon-29 Nuclear Magnetic Resonance Study of Silica. *J. Am. Chem. Soc.* **1992**, *112*, 6412–6418. [CrossRef]

54. Malfait, W.J.; Halter, W.E.; Verel, R. ^{29}Si NMR spectroscopy of silica glass: T1 relaxation and constraints on the Si–O–Si bond angle distribution. *Chem. Geol.* **2008**, *256*, 269–277. [CrossRef]

55. Baccile, N.; Laurent, G.; Bonhomme, C.; Innocenzi, P.; Babonneau, F. Solid-State NMR Characterization of the Surfactant-Silica Interface in Templated Silicas: Acidic versus Basic Conditions. *Chem. Mater.* **2007**, *19*, 1343–1354. [CrossRef]

56. Klinowski, J. Solid-State NMR Studies of Molecular Sieve Catalysts. *Chem. Rev.* **1991**, *91*, 1459–1479. [CrossRef]

57. Smith, K.A.; Kirkpatrick, R.J.; Oldfield, E.; Henderson, D.M. High-resolution silicon-29 nuclear magnetic resonance spectroscopic study of rock-forming silicates. *Am. Mineral.* **1983**, *68*, 1206–1215.

58. Li, J.; Hayakawa, S.; Shirosaki, Y.; Osaka, A. Revisiting structure of silica gels from water glass: An ^{1}H and ^{29}Si MAS and CP-MAS NMR study. *J. Sol.-Gel Sci. Technol.* **2013**, *65*, 135–142. [CrossRef]

59. Myers, S.A.; Cygan, R.T.; Assink, R.A.; Boslough, M.B. ^{29}Si MAS NMR relaxation study of shocked Coconino Sandstone from Meteor Crater, Arizona. *Phys. Chem. Miner.* **1998**, *25*, 313–317. [CrossRef]

60. Barron, P.F.; Frost, R.L.; Skjemstad, J.O. ^{29}Si Spin–lattice relaxation in aluminosilicates. *J. Chem. Soc. Chem. Commun.* **1983**, *10*, 581–583. [CrossRef]

61. Narayanan, A.; Hartman, J.S.; Bain, A.O. Characterizing Nonexponential Spin-Lattice Relaxation in Solid-State NMR by Fitting to the Stretched Exponential. *J. Magn. Reson. A* **1995**, *112*, 58–65. [CrossRef]

62. Peyron, M.; Pierens, G.K.; Lucas, A.J.; Hall, L.D.; Stewart, R.C. The Modified Stretched-Exponential Model for Characterization of NMR Relaxation in Porous Media. *J. Magn. Reson. Ser. A* **1996**, *118*, 214–220. [CrossRef]

63. Alaimo, M.H.; Roberts, J.E. Effects of paramagnetic cations on the nonexponential spin-lattice relaxation of rare spin nuclei in solids. *Solid State Nucl. Magn. Reson.* **1997**, *8*, 214–250. [CrossRef]

64. Leonova, E.; Grins, J.; Shariatgorji, M.; Ilag, L.L.; Edén, M. Solid-state NMR investigationsof Si-29 and N-15 enriched silicon nitride. *Solid State Nucl. Magn. Reson.* **2009**, *36*, 11–18. [CrossRef]

65. Watanabe, T.; Shimizu, H.; Masuda, A.; Saito, H. Studies of ^{29}Si spin-lattice relaxation times and paramagnetic impurities in clay minerals by magic-angle spinning ^{29}Si-NMR and EPR. *Chem. Lett.* **1983**, *12*, 1293–1296. [CrossRef]

66. Miró, J.; Martín-Martín, J.D.; Ibáñez, J.; Anadón, P.; Oms, O.; Tritlla, J.; Caja, M.A. Opaline chert nodules in maar lake sediments from Camp dels Ninots (La Selva Basin, NE Spain). *Teo-Gemas* **2016**, *16*, 387–390.

67. Liesegang, M.; Milke, R. Silica colloid ordering in a dynamic sedimentary environment. *Minerals* **2018**, *8*, 12. [CrossRef]

68. Jochum, K.P.; Nohl, U.; Herwig, K.; Lammel, E.; Stoll, B.; Hofmann, A.W. GeoReM: A New Geochemical Database for Reference Materials and Isotopic Standards. *Geostand. Geoanal. Res.* **2005**, *29*, 333–338. [CrossRef]

69. Struppe, J.; Steuernagel, S.; Aussenacc, F.; Benevelli, F.; Gierth, P.; Wegner, S. *Solid State NMR AVANCE Solids User Manual 003*; Bruker Corporation: Billerica, MA, USA, 2016.

70. Hayashi, S.; Hayamizu, K. Chemical Shift Standards in High-Resolution Solid-State NMR (1) ^{13}C, ^{29}Si and ^{1}H Nuclei. *Bull. Chem. Soc. Jpn.* **1991**, *64*, 685–687. [CrossRef]

71. Edwards, C.L.; Alemany, L.B.; Barron, A.R. Solid-State ^{29}Si NMR Analysis of Cements: Comparing Different Methods of Relaxation Analysis for Determining Spin−Lattice Relaxation Times to Enable Determination of the C3S/C2S Ratio. *Ind. Chem. Eng. Res.* **2007**, *46*, 5122–5130. [CrossRef]

72. Oster, J.L.; Kitajima, K.; Valley, J.; Rogers, B.; Maher, K. An evaluation of paired δ^{18}O and $(^{234}\text{U}/^{238}\text{U})_0$ in opal as a tool for paleoclimate reconstruction in semi-arid environments. *Chem. Geol.* **2017**, *449*, 236–252. [CrossRef]

73. Johnston, D.C. Stretched exponential relaxation arising from a continuous sum of exponential decays. *Phys. Rev. B* **2006**, *74*, 184430–184437. [CrossRef]

74. Press, W.H.; Flannery, B.P.; Teukolsky, S.A.; Vetterling, W.T. *Numerical Recipes The Art of Scientific Computing (Fortran Vesion)*; Cambridge University Press: Cambridge, UK, 1989.

75. Graetsch, H.; Topalovic, I.; Gies, H. NMR spectra of moganite and chalcedony. *Eur. J. Mineral.* **1994**, *6*, 459–464. [CrossRef]

76. Thomas, P.; Chauviré, B.; Flower-Donaldson, K.; Aldridge, L.; Smallwood, A.; Liu, B. FT-NIR and DSC characterisation of water in opal. *Ceram. Int.* **2020**, *46*, 29443–29450. [CrossRef]

77. Brown, L.D.; Ray, A.S.; Thomas, P.S. Elemental Analysis of Australian amorphous banded opals by laser-ablation ICP-MS. *Neues Jahrb. Mineral. Mon.* **2004**, *2004*, 411–424. [CrossRef]

78. Bartoli, F.; Rosa, D.B.; Doirisse, M.; Meyer, R.; Philippy, R.; Samama, J.-C. Role of aluminium in the structure of Brazilian opals. *Eur. J. Mineral.* **1990**, *2*, 611–619. [CrossRef]

79. Smallwood, A. A new era for opal nomenclature. *Aust. Gemmol.* **1997**, *19*, 489–496.

80. Megaw, P.K.M.; Fritsch, E.; Spano, T.L.; Gray, M. Geology and Mineralogy of Electric Opal$^{\text{TM}}$: Green Daylight-Luminescing Hyalite Opal from Zacatecas, Mexico. *Rocks Miner.* **2018**, *93*, 404–413. [CrossRef]

81. Gaillou, E. An Overview of Gem Opals: From the Geology to Color and Microstructure. In Proceedings of the Thirteenth Annual Sinkankas Symposium—Opal, Carlsbad, CA, USA, 18 April 2015.

82. Vasil'ev, S.G.; Volkov, V.I.; Tatarinova, E.A.; Muzafarov, A.M. A Solid-State NMR Investigation of MQ Silicone Copolymers. *Appl. Magn. Reson.* **2003**, *44*, 1015–1025. [CrossRef]

83. Bronnimann, C.E.; Zeigler, R.C.; Maciel, G.E. Proton NMR Study of Dehydration of the Silica Gel Surface. *J. Am. Chem. Soc.* **1988**, *110*, 2023–2026. [CrossRef]

84. Lowe, I.J.; Tse, D. Nuclear Spin-Lattice Relaxation via Paramagnetic Centers. *Phys. Rev.* **1968**, *166*, 279–291. [CrossRef]

85. Tse, D.; Hartmann, S.R. Nuclear spin-lattice relaxation via paramagentic centers without spin diffusion. *Phys. Rev. Lett.* **1968**, *21*, 511–514. [CrossRef]

86. Maiti, B.; McGarvey, B.R. Spin-Lattice Relaxation Time of ^{13}C in [Fe(phen)$_2$(N^{13}CS)$_2$]. Nonexponential Decay. *J. Magn. Reson.* **1984**, *58*, 37–46. [CrossRef]

87. Johnston, D.C.; Baek, S.-H.; Zong, X.; Borsa, F.; Schmalian, J.; Kondo, S. Dynamics of Magnetic Defects in Heavy Fermion LiV$_2$O$_4$ from Stretched Exponential ^{7}Li NMR Relaxation. *Phys. Rev. Lett.* **2005**, *95*, 176408. [CrossRef]

88. Belton, D.J.; Deschaume, O.; Perry, C.C. An overview of the fundamentals of the chemistry of silica with relevance to biosilicification and technological advances. *FEBS J.* **2012**, *279*, 1710–1720. [CrossRef]

89. Pewkliang, B.; Pring, A.; Brugger, J. The formation of precious opal: Clues from the opalization of bone. *Can. Mineral.* **2008**, *46*, 139–149. [CrossRef]

90. Rey, P.F. Opalisation of the Great Artesian Basin (Central Australia): An Australian story with a Martian twist. *Aust. J. Earth Sci.* **2013**, *60*, 219–314. [CrossRef]

91. Gaillou, E.; Fritsch, E.; Aguilar-Reyes, B.; Rondeau, B.; Post, J.; Barreau, A.; Ostroumov, M. Common gem opal: An investigation of micro- to nano-structure. *Am. Mineral.* **2008**, *93*, 1865–1873. [CrossRef]